in inducing MHC class I-mediated antitumor immunity. Although electroporation is commonly utilized as gene delivery method and deliver gene such as DNA and RNA into cytosol, Kim K.W. et al and Weiss J.M. et al. apply this system to antigen delivery into DCs [10,11]. Their reports also demonstrate the importance of delivering exogenous antigens into cytosol of DCs to induce MHC class I presentation of the antigens.

It has been reported that ultrasound (US) increases the permeability of the plasma membrane, which encourages the entry of DNA into cells [12,13]. The first studies applying US for gene delivery used frequencies in the range of 20–50 kHz [12,14]. However, these frequencies, along with cavitation, are also known to induce tissue damage if not properly controlled [15–17]. To address this problem, many studies into using therapeutic US for gene delivery have used frequencies of 1–3 MHz, intensities of 0.5–2.5 W/cm^2 and a pulse-mode [18–20]. In addition, it was reported that the combination of therapeutic US and microbubble echo contrast agents could enhance gene transfection efficiency [21–27]. In this method, DNA is effectively and directly transferred into the cytosol. This system has been applied to deliver proteins into cells [28,29], but not yet to deliver antigens into DCs for the purpose of cancer immunotherapy. Previously, we developed novel liposomal bubbles containing nanobubbles of the US imaging gas, perfluoropropane [30–34] and suggested that these "Bubble liposomes" (BLs) might be used as novel non-viral gene delivery tools if combined with US exposure. In the case of DCs, the antigen delivered into the cytosol would present on MHC class I molecules and result in priming antigen-specific CTLs. In this study, we examined the effectiveness of BLs combined with US exposure to deliver antigen into DCs. In addition, the effectiveness of this antigen delivery system in DC-based cancer immunotherapy was assessed.

2. Materials and methods

2.1. Cells

T cell hybridoma CD8-OVA1.3 (a kind gift from Dr. C.V. Harding, Department of Pathology, Case Western Reserve University, Cleveland, OH, USA), a cell type that recognizes SIINFEKL:H-2K^b complexes [35], was cultured in Dulbecco's modified Eagle's medium (DMEM, Sigma Chemical Co., St. Louis, MO, USA) supplemented with 10% heat inactivated fetal bovine serum (FBS, GIBCO, Invitrogen Co., Carlsbad, CA, USA), 50 μM 2-mercaptethanol (2-ME), 250 μg/ml amphotericin B (Wako Pure Chemical Industries, Ltd., Osaka, Japan) and 50 μg/ml gentamycin (Wako Pure Chemical Industries). EL-4 murine thymoma cells were cultured in RPMI 1640 supplemented with 10% FBS and 50 μM 2-ME. E.G7-OVA cells (OVA cDNA transfectant of EL4 cells) were maintained in RPMI 1640 supplemented with 10% FBS, 50 μM 2-ME and 400 μg/ml GENETICIN (G418 sulfate, GIBCO, Invitrogen). All culture media contained 50 U/ml penicillin and 50 μg/ml streptomycin (Wako Pure Chemical Industries).

2.2. Generation of mouse bone marrow-derived DCs

DCs were generated from bone marrow cells as described elsewhere [36]. Briefly, bone marrow cells were isolated from C57BL/6 mice and were cultured in RPMI 1640 with 10% FBS, 50 U/ml penicillin, 50 μg/ml streptomycin and 40 ng/ml mouse granulocyte-macrophage colony-stimulating factor (GM-CSF). After 8–16 days of culture, non-adherent cells were collected and used as DCs.

2.3. Preparation of BLs

Liposomes composed of 1,2-distearoyl-sn-glycero-phosphatidylcholine (DSPC) (NOF Corp., Tokyo, Japan) and 1,2-distearoyl-sn-glycero-3-phosphatidyl-ethanolamine-methoxypolyethyleneglycol (DSPE-PEG(2k)-OMe, (PEG Mw=ca. 2000), NOF) (94 : 6 (m/m)) were prepared by reverse phase evaporation. Briefly, all reagents (total lipid: 100 μmol) were dissolved in 8 ml of 1:1 (v/v) chloroform/diisopropyl ether, then 4 ml of phosphate buffered saline (PBS) was added. The mixture was sonicated and evaporated at 65 °C. The solvent was completely removed, and the size of the liposomes was adjusted to less than 200 nm using an extruding apparatus (Northern Lipids Inc., Vancouver, BC, Canada) and sizing filters (pore sizes: 100 and 200 nm; Nuclepore Track-Etch Membrane, Whatman plc, UK). After sizing, the liposomes were sterilized by passing them through a 0.45 μm pore size filter (MILLEX HV filter unit, Durapore PVDF membrane, Millipore Corp., MA, USA). The size of the liposomes was measured by dynamic light scattering (ELS-800, Otsuka Electronics Co., Ltd., Osaka, Japan). The average diameter of these liposomes was between 150–200 nm. Lipid concentration was measured using the Phospholipid C test (Wako Pure Chemical Industries). BLs were prepared from the liposomes and perfluoropropane gas (Takachiho Chemical Industrial Co., Ltd., Tokyo, Japan) [31,33]. Briefly, 5 ml sterilized vials containing 2 ml of the liposome suspension (lipid concentration: 2 mg/ml) were filled with perfluoropropane, capped, and then supercharged with 7.5 ml of perfluoropropane. The vial was placed in a bath-type sonicator (42 kHz, 100 W; BRANSONIC 2510J-DTH, Branson Ultrasonics Co., Danbury, CT, USA) for 5 min to form the BLs. In this method, the liposomes were reconstituted by sonication under the condition of supercharge with perfluoropropane in the 5 mL vial container. At the same time, perfluoropropane would be entrapped within lipids like micelles, which were made by DSPC and DSPE-PEG(2k)-OMe from liposome composition, to form nanobubbles. The lipid nanobubbles were encapsulated within the reconstituted liposomes, which sizes were changed into around 1 μm from 150–200 nm of original.

2.4. Antigen trafficking into DCs after antigen delivery with BLs and US exposure

Alexa Fluor 488 conjugated OVA (Alexa-OVA) was prepared with Alexa Fluor 488 succinimidyl ester (Molecular Probes, Invitrogen) according to the instruction manual. DCs (1×10^5 cells/ml) were cultured in a glass bottom dish (IWAKI, Asahi Glass Co. Ltd., Tokyo, Japan) overnight. After washing the cells with OptiMEM (Invitrogen), BLs (240 μg/ml) and Alexa-OVA (50 μg/ml) were added to the dish. Then, the DCs were exposed to US exposure (frequency: 2 MHz, duty: 10%, burst rate: 2.0 Hz, intensity 2.0 W/cm^2, time: 3×10 s (interval: 10 s)) using a Sonopore 4000 (6 mm diameter probe; Nepa Gene Co. Ltd., Chiba, Japan). This condition was decided referring to our reports about gene delivery [31,33] and Guo et al.'s report about the repeat US exposure with interval [37], and from the viewpoint of cytotoxicity for DCs. After US exposure, the DCs were incubated for 1 h at 37 °C, then washed with PBS, fixed with 3% paraformaldehyde for 10 min, and treated with 0.1% Triton X-100 (Wako Pure Chemical Industries) for 5 min. In addition, some DCs were washed with PBS, their nuclei were stained with propidium iodide (0.5 μg/ml) (Wako Pure Chemical Industries), and antigen trafficking was observed with a confocal laser microscope.

2.5. Antigen delivery following inhibition of the endocytosis pathway in DCs

DCs were pretreated with OptiMEM containing 10 mM NaN_3 for 1 h at 4 °C to inhibit the endocytosis pathway. After washing the cells, BLs (240 μg/ml) and Alexa-OVA (50 μg/ml) were added to the DCs in OptiMEM containing 10 mM sodium azide (NaN_3). The DCs were exposed to US exposure (frequency: 2 MHz, duty: 10%, burst rate: 2.0 Hz, intensity 2.0 W/cm^2, time: 3×10 s (interval: 10 s)), then washed with PBS containing10 mM NaN_3. After US exposure, DCs were fixed and their nuclei were stained as described above (2.4.).

2.6. Flow cytometry analysis of antigen delivery into DCs with BLs and US exposure

Alexa-OVA was delivered into DCs under inhibited endocytosis conditions as described above (2.5.). After washing, the DCs were stained with propidium iodide (100 ng/ml) and analyzed by flow cytometry (FACSCalibur, Becton, Dickinson and Company, Franklin Lakes, NJ, USA). In this study, living DCs (1×10^4 cells) were analyzed by gating out propidium iodide staining cells.

2.7. Assessment of MHC class I restricted OVA presentation

DCs (2.5×10^5 cells/500 μl/well (48-well plate)) were pulsed with OVA alone (0, 10, 100, 1000 μg/ml) or OVA (0, 10, 100, 1000 μg/ml) using US exposure (frequency: 2 MHz, duty: 10%, burst rate: 2.0 Hz, intensity 2.0 W/cm^2, Time: 3×10 s (interval: 10 s)) and/or BLs (240 μg/ml). After US exposure, the DCs were incubated for 1 h at 37 °C, then washed with PBS. After culturing for 24 h, the DCs were co-cultured for 20 h with T cell hybridoma CD8-OVA1.3 (2×10^5 cells/well) that recognizes SIINFEKL: H-2K^b complexes. The concentration of IL-2 in the supernatants was measured using an IL-2 ELISA Kit (BioSource International, Inc., Camarillo, CA, USA).

2.8. Assessment of cytotoxicity to DCs by the treatment of BLs and US exposure

DCs (2.5×10^5 cells/500 μl/well (48-well plate)) were treated with BLs (240 μg/ml) and/or US exposure (frequency: 2 MHz, duty: 10%, burst rate: 2.0 Hz, intensity 2.0 W/cm^2, Time: 3×10 s (interval: 10 s)). After US exposure, DCs were incubated for 1 h at 37 °C, and washed with PBS. The DCs were resuspended with cuture medium (250 μl) and cultured for 48 h. Cell viability was assayed using MTT (3-(4,5-s-dimethylthiazol-2-yl)-2,5-diphenyl tetrazolium bromide, Dojindo, Kumamoto, Japan) as described by Mosmann with minor modifications [38]. Briefly, MTT (5 mg/mL, 25 μL) was added to each well and the cells were incubated at 37 °C for 4 h. The formazan product was dissolved in 250 μL of 10% sodium dodecyl sulfate (SDS, Wako Pure Chemical Ind. Co., Ltd. Osaka, Japan) containing 15 mM HCl. Color intensity was measured using a microplate reader (POWERSCAN HT; Dainippon Pharmaceutical, Osaka, Japan) at test and reference wavelengths of 595 and 655 nm, respectively.

2.9. Immunization of mice with DCs and cytotoxicity assay

DCs (2.5×10^5 cells/500 μl/well) were pulsed with OVA alone (100 μg/ml) or OVA (100 μg/ml) using US exposure (frequency: 2 MHz, duty: 10%, burst rate: 2.0 Hz, intensity 2.0 W/cm^2, Time: 3×10 s (interval: 10 s)) and/or BLs (240 μg/ml) on a 48-well plate, then collected from 10 wells and seeded into 6-well plates. After 1 h incubation at 37 °C, the DCs were washed and cultured for 24 h at 37 °C. After washing, DCs (1×10^6 cells/100 μl) were intradermally injected into the backs of C57BL/6 mice. After 7 days, the mice were re-immunized. Seven days after the second immunization, splenocytes were obtained from five mice, and the splenocytes were pooled and stimulated with mitomycin C-treated E.G7-OVA cells at a ratio of 10:1 for 5 days. The stimulated splenocytes were used as effector cells for the cytotoxicity assay, using EL-4 or E.G7-OVA as the target cells in a flow cytometric assay employing two fluorochromes [39]. PKH-67, a fluorochrome which fluoresces green, binds to the cytoplasmic membrane and does not leak or transfer, was used to identify the target cell population. Propidium iodide fluoresces red and was used to detect non-viable cells. Use of these two fluorochromes and two parameter analyses allowed the identification of four subpopulations in the sample: live effectors, dead effectors, live targets and dead targets. By enumerating these subpopulations, the percent target lysis can be calculated.

2.10. Antitumor effect by prior immunization with antigen-pulsed DCs

DCs (2.5×10^5 cells/500 μl/well) were pulsed with OVA alone (100 μg/ml) or OVA (100 μg/ml) using US exposure (frequency: 2 MHz, duty: 10%, burst rate: 2.0 Hz, intensity 2.0 W/cm^2, Time: 3×10 s (interval: 10 s)) and/or BLs (240 μg/ml) on a 48-well plate, then collected from 10 wells and seeded into 6-well plates. After 1 h incubation at 37 °C, the DCs were washed and cultured for 24 h at 37 °C. After washing, the DCs (1×10^6 cells/100 μl) were intradermally immunized into the backs of C57BL/6 mice twice at intervals of one week. Seven days after the second immunization, E.G7-OVA cells (1×10^6 cells) were intradermally inoculated into the backs of mice and the size of the tumors was monitored using the formula: (major axis×minor axis^2)×0.5. All treated groups contained five mice.

2.11. Re-challenge of tumor cells

E.G7-OVA cells (1×10^6 cells) were injected into mice that were resistant to tumor cells due to immunization with DCs treated with BLs, US exposure and OVA. Untreated mice were used as controls to confirm the development of cancer following the first inoculation with E.G7-OVA cells. All treated groups contained five mice.

2.12. Treatment of tumor-bearing mice with antigen-pulsed DCs

E.G7-OVA cells (1×10^6 cells) were intradermally inoculated into the backs of C57BL/6 mice. On day 9, when the tumors were between 8–10 mm, OVA pulsed DCs (1×10^6 cells) prepared as described above were intradermally injected into the backs of the mice. On day 12, DCs were injected similarly. Tumor sizes were monitored from the day of inoculation. All treated groups contained five mice.

2.13. Statistical analysis

Differences in IL-2 secretion between the experimental groups were compared using non-repeated measures ANOVA and Dunnett's test.

3. Results

3.1. Antigen delivery by BLs and sonoporation into the cytosol of DCs lacking the endocytosis pathway

We examined antigen trafficking following delivery using a combination of BLs and US exposure (Fig. 1(a)). In DCs treated with Alexa-OVA in the presence or absence of either BLs or US exposure, the fluorescence from Alexa-OVA appeared as dots in the cytosol. On the other hand, in DCs treated with Alexa-OVA, BLs and US exposure, the fluorescence appeared as dots, but also as diffused fluorescence in the cytosol. To confirm this, antigen delivery was examined following inhibition of the endocytosis pathway in DCs by treatment with sodium azide (Fig. 1(b)). In DCs treated with Alexa-OVA either with or without BLs or US exposure, the fluorescence derived from Alexa-OVA was not observed. On the other hand, in DCs treated with Alexa-OVA, BLs and US exposure, fluorescence was observed in the cytosol even when the endocytosis pathway in DCs was inhibited. In addition, the efficiency of antigen delivery following inhibition of the endocytosis pathway was assessed using flow cytometory (Fig. 1(c)). The fluorescence intensity of DCs treated with Alexa-OVA, BLs and US exposure was higher than that of DCs treated with Alexa-OVA alone, or of Alexa-OVA and BLs or US exposure. These data support the data shown in Fig. 1(b), indicating that Alexa-OVA is observed in the cytosol when DCs are only treated with BLs and US exposure, even when the endocytosis pathway is

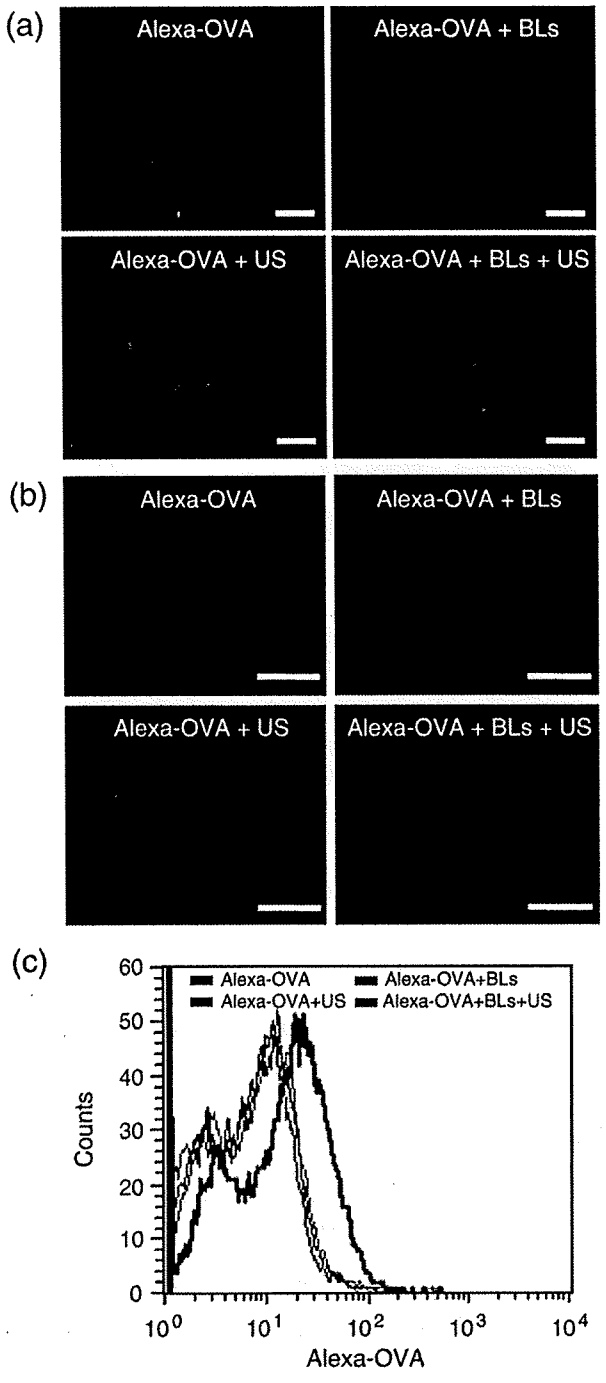

Fig. 1. Intracellular antigen delivery into DCs using BLs and US exposure. (a) Uptake of Alexa-OVA into DCs. DCs were cultured in a glass bottom dish overnight. After washing the cells, Alexa-OVA was added to the dish. Then, the DCs were exposed to US in the presence or absence of BLs and incubated for 1 h at 37 °C. The DCs were washed with PBS, fixed, and the nuclei were stained with propidium iodide. The uptake of Alexa-OVA was observed using a confocal laser microscope. (b) Intracellular delivery of Alexa-OVA into DCs using BLs and US. DCs were pretreated with OptiMEM containing 10 mM NaN_3 for 1 h at 4 °C to inhibit the endocytosis pathway. After washing the cells, Alexa-OVA was added to the DCs in OptiMEM containing10 mM NaN_3. Then, the DCs were exposed to US in the presence or absence of BLs. After US exposure, the DCs were washed with PBS containing 10 mM NaN_3, fixed, and the nuclei were stained with propidium iodide. Intracellular trafficking of Alexa-OVA in the DCs was observed using a confocal laser microscope. Scale bar shows 5 μm. (c) Flow cytometry analysis of DCs containing Alexa-OVA delivered using BLs and US. Alexa-OVA was delivered into the cell interior of the DCs during endocytosis inhibition. After washing the cells, the DCs were analyzed by flow cytometry.

inhibited. These results suggest that the combination of BLs and US exposure can be used to directly deliver antigens into the cytosol of DCs in the absence of endocytosis.

3.2. MHC class I presentation of exogenous antigen delivered into DCs by BLs and US exposure

Exogenous antigen delivered into the cytosol of DCs by BLs and US exposure is recognized as endogenous antigen by DCs and leads to the efficient presentation of peptides derived from exogenous antigens on MHC class I molecules. Thus, we examined whether antigen delivery by BLs and US exposure resulted in the efficient presentation of peptides on MHC class I molecules and the stimulation of $CD8^+$ T cells. C57BL/6-derived OVA-specific T cell hybridoma CD8-OVA1.3 was co-cultured with mouse bone marrow-derived DCs pulsed with antigen. As shown in Fig. 2, CD8-OVA1.3 cells stimulated with DCs pulsed with soluble OVA, either treated or untreated by BLs or US exposure did not secrete a significant amount of IL-2. Of note, a larger amount of IL-2 was secreted by CD8-OVA1.3 cells stimulated with DCs pulsed with OVA treated with a combination of BLs and US exposure. These data indicate that antigen delivery by BLs to DCs upon sonoporation results in the presentation of peptides derived from OVA on MHC class I molecules. In this data, the level of IL-2 secretion increased depending on OVA concentration and reached plateau in 100 μg/ml of OVA concentration. Therefore, we used this OVA concentration (100 μg/ml) in further examinations.

3.3. Cytotoxicity to DCs by the treatment of BLs and US exposure

In this antigen delivery system using BLs and US exposure, the transient pores would be provided on the membrane of DCs. Therefore, it is concerned that the DCs are injured by US exposure in the presence of BLs. To assess the cytotoxicity to DCs by the treatment of BLs and US exposure, we examined about the viability of DCs (Fig. 3). In the treatment of DC with BLs and/or US exposure, the viability of DCs treated with BLs, US exposure or BLs/US exposure was 83 ± 11%, 96 ± 5% or 87 ± 13%, respectively. This result shows that there is not serious damage to DCs even under the condition of inducing transient pores on the membrane of DCs treated with BLs and US exposure.

3.4. Induction of antigen-specific CTL response in the immunization of DCs pulsed with antigen using BLs and US exposure

To examine whether efficient peptide presentation on MHC class I molecules leads to strong induction of antigen-specific CTLs *in vivo*, we immunized C57BL/6 mice twice with bone marrow-derived DCs that had been treated with various antigen delivery techniques. Thereafter, splenocytes were isolated, and a cytotoxicity assay was

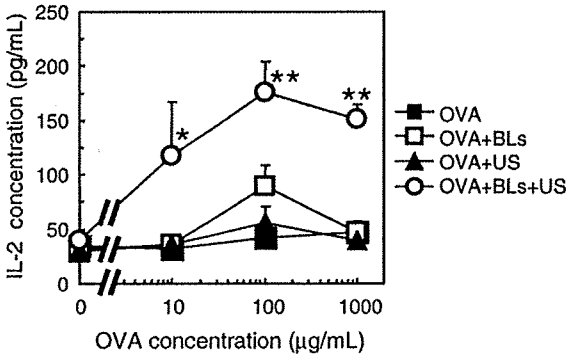

Fig. 2. MHC class I restricted OVA presentation after OVA delivery into DCs using a combination of BLs and US exposure. DCs were pulsed with OVA alone or OVA in conjunction with US exposure and/or BLs. After US exposure, the DCs were incubated for 1 h at 37 °C, then washed with PBS. After culturing for 24 h, the DCs were co-cultured with CD8-OVA1.3 cells for 20 h. The concentration of IL-2 in the supernatants was measured. Each data represents the mean±S.D. for triplicate measurements. *$P<0.05$ compared to the group treated with BLs or US, or without BLs and US. **$P<0.01$ compared to the group treated with BLs or US, or without BLs and US.

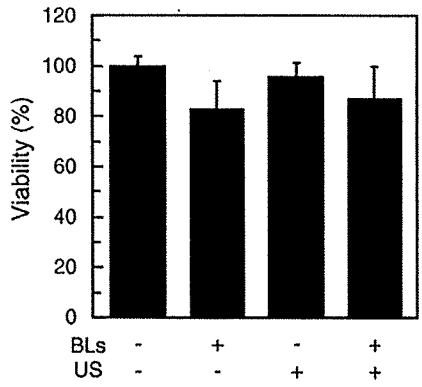

Fig. 3. Viability of DCs treated with BLs and /or US exposure. DCs were treated with BLs and/or US. After US exposure, DCs were incubated for 1 h at 37 °C, then washed with PBS. After culturing for 48 h, the viability of DCs was measured by MTT assay. Each data represents the mean±S.D. for triplicate measurements.

performed using the syngeneic lymphoma cell line EL-4 or its OVA transfectant, E.G7-OVA. As shown in Fig. 4, immunization with DCs without OVA, DCs pulsed with OVA, or OVA combined with BLs or US exposure, induced weak cytotoxicity of splenocytes against the OVA-expressing cell line E.G7-OVA. In contrast, immunization with DCs pulsed with OVA following BL and US exposure resulted in strong cytotoxicity against the OVA-expressing cell line E.G7-OVA by splenocytes. Splenocytes from mice immunized with DCs pulsed using any method of antigen delivery did not exhibit strong cytotoxicity against the parental cell line EL-4. These data indicate that DCs pulsed with antigen using BLs and US exposure as the antigen delivery method efficiently present peptides on MHC class I molecules, which results in strong induction of antigen-specific CTLs *in vivo*.

3.5. Antitumor effects in the immunization of DCs pulsed with antigen by BLs and US exposure

Using an E.G7-OVA tumor model, we examined whether the strong induction of CTLs by antigen delivery with BLs and US exposure leads to efficient anti-tumor immune responses *in vivo*. We immunized C57BL/6 mice twice with bone marrow-derived DCs that had been pulsed using one of two methods of antigen delivery (OVA with US exposure, or OVA with BLs and US exposure). One week after the second immunization, the mice were inoculated intradermally with E.G7-OVA cells, and tumor growth was monitored. As shown in Fig. 5(a) and (b), immunization with untreated DCs weakly suppressed tumor growth. The survival rate of mice immunized with untreated DCs was slightly prolonged, suggesting that non-specific inflammatory responses induced by the injection of DCs result in weak anti-tumor immune responses. Immunization with DCs that had been pulsed with OVA using US exposure suppressed tumor growth slightly more efficiently than the control immunization. Of note, immunization with DCs that had been pulsed with OVA using BLs and US exposure completely suppressed tumor growth, with all mice in this group surviving more than 70 days after tumor inoculation. In addition, we examined the prevention of tumor growth recurrence after re-inoculation of tumor cells into mice, which had completely rejected the first injection of tumor cells (Fig. 5(c)). All mice, which were re-inoculated with E.G7-OVA cells 10 weeks after the first inoculation, completely rejected the tumor cells.

Finally, we examined whether immunization with DCs pulsed with antigen using BLs and US exposure can efficiently suppress the growth of established tumors. For this purpose, we inoculated C57BL/6 mice with E.G7-OVA, and after 9 and 12 days, when the tumors were between 100–200 mm^3, DCs were injected intradermally. As shown in Fig. 6(a), administration of untreated DCs did not provide a significant therapeutic effect. Administration of DCs pulsed with OVA using US exposure exhibited a weak therapeutic effect. Importantly, administration of DCs pulsed with OVA using BLs and US exposure exhibited stronger therapeutic effects in two of the five mice, with these two mice surviving for more than 60 days (Fig. 6(b)). These data indicate that antigen delivery into DCs with BLs and US exposure can induce significant therapeutic effects on established tumors.

4. Discussion

Subunit vaccines utilizing MHC class I-binding peptides have significant limitations that hinder their application to the general patient population (restrictions of HLA types) and that also affect their clinical effectiveness (monovalency of tumor specific antigen) in DC-based tumor immunotherapy. Utilization of tumor associated proteins as antigens may overcome this limitation, thereby enabling a broad spectrum of peptide presentation. In fact, patients treated with tumor cell lysates pulsed DCs showed better response rates compared with patients treated with peptide pulsed DCs [40]. This clinical trial suggests that tumor lysates are a good source of tumor antigens for a polyvalent antitumor vaccine. On the other hand, MHC class I molecules generally present endogenous antigens, whereas exogenous antigens for DCs are taken up by the endocytosis pathway and exogenous antigen-derived peptides are presented on MHC class II molecules [3]. In this study, we showed that by using a combination of BLs and US exposure, exogenous antigen was directly delivered into the cytosol of DCs (Fig. 1) and was presented on MHC class I molecules (Fig. 2). In addition, DCs immunized with antigen delivered by BLs and US exposure could stimulate antigen-specific CTL activation (Fig. 4) and resulted in inducing effective anti-tumor immune responses in tumor-bearing mice. (Figs. 5 and 6) Although peptide and protein delivery with sonoporation using microbubbles have been previously reported [28,29,41], the present study is the first report of effective antigen delivery into DCs by BLs using sonoporation for cancer immunotherapy.

Sonoporation and microbubbles such as Optison have been reported to be an effective gene delivery method using non-viral vectors. In addition, peptide and protein delivery with microbubbles and US exposure has been reported [28,29,41]. In the reports, Bekeredjian et al. showed the feasibility of microbubbles and US exposure for delivery of bioactive protein (luciferase, 60 kDa) into the cytosol of *in vitro* and *in vivo* cells [28,29]. Larina I.V. et al. reported that FITC-dextrans of 10–2000 kDa were delivered into human breast

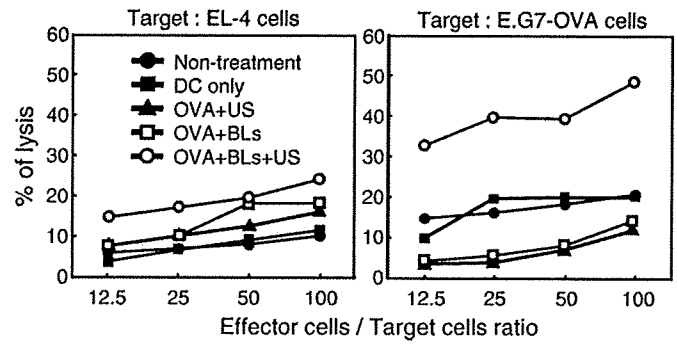

Fig. 4. Antigen specific CTL induction after immunization with DCs treated with BLs and US exposure. DCs were pulsed with OVA under each condition and cultured. After washing the cells, the DCs were intradermally injected into the backs of C57BL/6 mice. After 7 days, the mice were re-immunized. Seven days after the second immunization, splenocytes were obtained and stimulated with mitomycin C-treated E.G7-OVA cells at a ratio of 10:1 for 5 days. The stimulated splenocytes were used as effector cells for a cytotoxicity assay, using EL-4 or E.G7-OVA cells as the target in a flow cytometric assay.

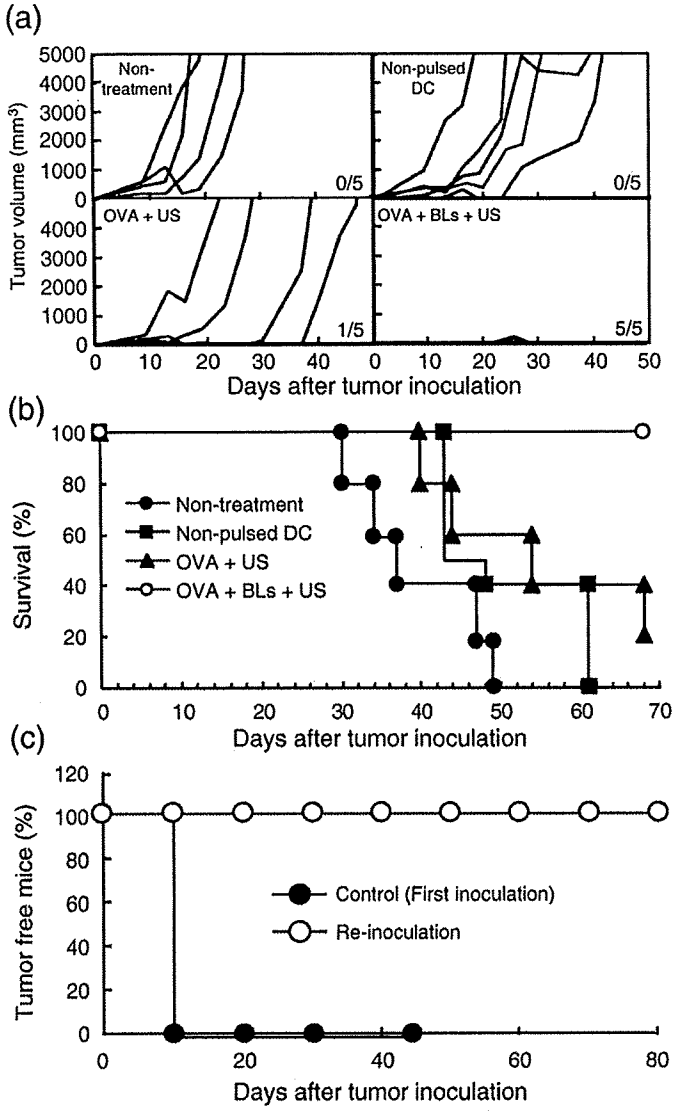

Fig. 5. Antitumor effect caused by immunization of DCs treated with antigen, BLs and US exposure. C57BL/6 mice were immunized with DCs twice. Seven days after the second immunization, E.G7-OVA cells were intradermally inoculated into the backs of the mice, and the tumor volume and survival of the mice was monitored. (a): Tumor volume of the mice after tumor inoculation. Each line indicates the tumor volume in an individual mouse. The fractional number in the lower right of each group shows the number of mice completely rejecting tumors / the number of total experimental mice. (b): Survival rate of the mice after tumor inoculation. (c): Tumor rejection efficiency after re-inoculation with tumor cells. E.G7-OVA cells were re-injected into the mice, which had rejected tumor cells following immunization with DCs treated with OVA, BLs and US in a prior immunization (a). Normal mice were used as controls to confirm the development of cancer following the first inoculation with E.G7-OVA cells. All treated groups contained five mice.

adenocarcinoma (MCF7) by the combination of Optison (conventional microbubbles) and US exposure [42]. It is believed that the delivery mechanism is due to the presence of transient pores through the cell membrane, resulting in extracellular molecules being directly delivered into the cytosol [22,43]. As shown in Fig. 1(b), antigen was directly delivered into DCs by the combination of BLs and US exposure even when the endocytosis pathway was inhibited. Therefore, it is thought that the antigen delivery mechanism induced by BLs and sonoporation is the same as that induced by microbubbles and sonoporation. In studies using microbubbles and sonoporation, pore sizes (based on the physical diameter of the component compounds) were typically between 30–100 nm, and estimates of the membrane recovery time ranged from a few seconds to a few minutes [44]. On the other hand, in studies on the aftereffects of US exposure on cell membranes, Eshet *et al.* reported that microbubbles resulted in a rougher cell surface characterized by depressions, but that the effects are reversible within 24 h following US exposure [43]. In the present study, DCs were incubated with antigen for 1 h after US exposure and increased the delivery efficiency of antigen into the cytosol of DCs. We confirmed the efficiency of MHC class I antigen presentation in DCs with/without 1 h incubation after US exposure. The efficiency following 1 h incubation was higher than that without incubation (data not shown). This result suggests that the membrane permeability of DCs increases even after US exposure. Although the mechanism behind antigen delivery by BLs is unknown, our data support a temporary increase in permeability of the plasma membrane after US exposure. Moreover, recent data from microbubble studies suggest that the resealing of US-induced pores is an energy-dependent process, with the cells exhibiting morphological features consistent with an active and vesicle-based wound-healing responses [45]. Therefore, cells treated with sonoporation are viable due to this recovery mechanism. In this study, the viability of the DCs treated with BLs and US exposure was maintained more than 85% (Fig. 3). The accumulated evidence suggests that the combination of BLs and US exposure is an unique antigen delivery system which can deliver exogenous antigens into the cytosol without serious damage to DCs.

In this study, exogenous antigens, directly delivered into the cytosol of DCs by means of BLs and US exposure, were presented on MHC class I molecules. In addition, immunization of DCs treated with antigen, BLs and US exposure effectively primed antigen-specific CTLs. On the other hand, MHC class I antigen presentation lead to low-level

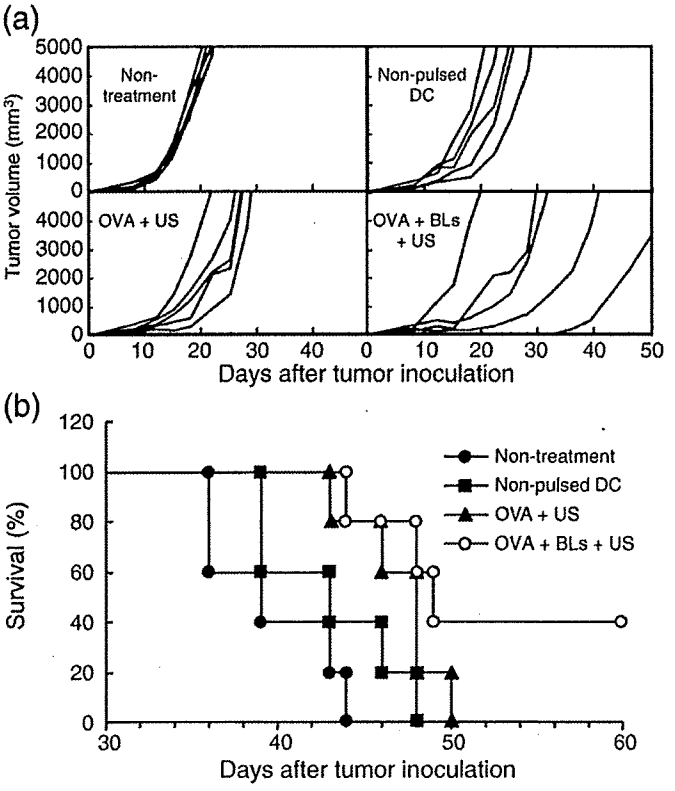

Fig. 6. Immunization of DCs treated with antigen, BLs and US exposure: therapeutic effect on tumor growth. E.G7-OVA cells were intradermally inoculated into the backs of C57BL/6 mice. On day 9, at a tumor size of 8–10 mm, OVA pulsed DCs were intradermally injected into the backs of the mice. On day 12, DCs were injected similarly. The tumor volume and survival of the mice was monitored. (a): Tumor volume of the mice after tumor inoculation. Each line indicates the tumor volume in individual mice. (b): Survival rate of the mice after tumor inoculation. All treated groups contained five mice.

antigen delivery with either BLs or US exposure. In these treated cells, antigen was mainly taken up via the endocytosis pathway. Although we have not confirmed MHC class II presentation, the antigen would presumably be presented on MHC class II molecules to DCs via the general antigen processing mechanism [10]. The exogenous antigens directly delivered into the cytosol would be processed similarly endogenously derived antigens, which are enzymatically digested into peptides, mainly by cytosolic proteases called proteasomes, and are then transported by transporters associated with antigen processing (TAP) molecules into the endoplasmic reticulum (ER). In the ER lumen, peptides bind to MHC class I molecules, which are subsequently transported via the Golgi apparatus to the cell surface [46]. Moreover, immunization of DCs treated with OVA, BLs and US exposure could prime OVA-specific CTLs. This result indicates that DCs presented with OVA-derived epitope peptides on MHC class I molecules effectively prime OVA-specific CTLs *in vivo*. We suspected that the effective priming of antigen-specific CTLs would result in the rejection of tumor cells. As shown in Fig. 5(a), all the immunized mice completely rejected the inoculated tumor cells. Tumor cells were intradermally re-injected into these mice to re-challenge their immune system and assess the preventive effects of immunization for suppressing tumor regeneration (Fig. 5(c)). Rejection following re-challenge with tumor cells suggests the induction of an antigen memory system in the host's immune system, i.e., memory T cells for the immunization antigen. Thus, this therapeutic method has potential for suppressing the regeneration and metastasis of tumors. Finally, we also assessed the therapeutic effects of this treatment towards established tumors (Fig. 6). Immunization with DCs treated with antigen, BLs and US exposure lead to significant therapeutic effects towards established tumors. Tumor cells generally secrete cytokines such as TGF-β to suppress the host's immune system. It is therefore possible that antigen delivery with BLs and US exposure could effectively induce an anti-tumor immune response even in the presence of established tumors.

In conclusion, we have developed a novel system for delivering antigens into DCs using BLs and sonoporation. Immunization of DCs using this antigen delivery system could effectively prime the anti-tumor immune system due to the induction of MHC class I TAA presentation. Therefore, BLs in conjunction with sonoporation might be a useful antigen delivery system for DC-based cancer immunotherapy. In the future, this system will be applied to various antigens containing unknown TAAs, such as crude antigens separated from surgically-removed human tumors.

Acknowledgments

The authors thank Mr. Shota Otake, Mr. Norihito Nishiie, Mr. Ken Osawa, Ms. Risa Koshima, Ms. Motoka Kawamura, Mr. Ryo Tanakadate, Mr. Kunihiko Matsuo and Mr. Yasuyuki Shiono (Teikyo University) for their technical assistance, and Mr. Yasuhiko Hayakawa, Mr. Takahiro Yamauchi and Mr. Kosho Suzuki (Nepa Gene Co., Ltd.) for their technical advice regarding US exposure. This study was supported by the Program for Promotion of Fundamental Studies in Health Sciences of the National Institute of Biomedical Innovation (NIBIO). Tetsuya Kodama acknowledges the Grant for Research on Nanotechnical Medical, the Ministry of Health, Labour and Welfare of Japan (H19-nano-010).

References

[1] F.O. Nestle, A. Farkas, C. Conrad, Dendritic-cell-based therapeutic vaccination against cancer, Curr. Opin. Immunol. 17 (2005) 163–169.
[2] J. Copier, A. Dalgleish, Overview of tumor cell-based vaccines, Int. Rev. Immunol. 25 (2006) 297–319.
[3] R.N. Germain, MHC-dependent antigen processing and peptide presentation: providing ligands for T lymphocyte activation, Cell 76 (1994) 287–299.
[4] P. Elamanchili, M. Diwan, M. Cao, J. Samuel, Characterization of poly(D,L-lactic-co-glycolic acid) based nanoparticulate system for enhanced delivery of antigens to dendritic cells, Vaccine 22 (2004) 2406–2412.
[5] T. Yoshikawa, N. Okada, A. Oda, K. Matsuo, K. Matsuo, Y. Mukai, Y. Yoshioka, T. Akagi, M. Akashi, S. Nakagawa, Development of amphiphilic gamma-PGA-nanoparticle based tumor vaccine: potential of the nanoparticulate cytosolic protein delivery carrier, Biochem. Biophys. Res. Commun. 366 (2008) 408–413.
[6] P. Machy, K. Serre, L. Leserman, Class I-restricted presentation of exogenous antigen acquired by Fcgamma receptor-mediated endocytosis is regulated in dendritic cells, Eur. J. Immunol. 30 (2000) 848–857.
[7] N. Okada, T. Saito, K. Mori, Y. Masunaga, Y. Fujii, J. Fujita, K. Fujimoto, T. Nakanishi, K. Tanaka, S. Nakagawa, T. Mayumi, T. Fujita, A. Yamamoto, Effects of lipofectin-antigen complexes on major histocompatibility complex class I-restricted antigen presentation pathway in murine dendritic cells and on dendritic cell maturation, Biochim. Biophys. Acta 1527 (2001) 97–101.
[8] L. Wang, H. Ikeda, Y. Ikuta, M. Schmitt, Y. Miyahara, Y. Takahashi, X. Gu, Y. Nagata, Y. Sasaki, K. Akiyoshi, J. Sunamoto, H. Nakamura, K. Kuribayashi, H. Shiku, Bone marrow-derived dendritic cells incorporate and process hydrophobized polysaccharide/oncoprotein complex as antigen presenting cells, Int. J. Oncol. 14 (1999) 695–701.
[9] K. Kawamura, N. Kadowaki, R. Suzuki, S. Udagawa, S. Kasaoka, N. Utoguchi, T. Kitawaki, N. Sugimoto, N. Okada, K. Maruyama, T. Uchiyama, Dendritic cells that endocytosed antigen-containing IgG-liposomes elicit effective antitumor immunity, J. Immunother. 29 (2006) 165–174.
[10] K.W. Kim, S.H. Kim, J.H. Jang, E.Y. Lee, S.W. Park, J.H. Um, Y.J. Lee, C.H. Lee, S. Yoon, S.Y. Seo, M.H. Jeong, S.T. Lee, B.S. Chung, C.D. Kang, Dendritic cells loaded with exogenous antigen by electroporation can enhance MHC class I-mediated antitumor immunity, Cancer Immunol. Immunother. 53 (2004) 315–322.
[11] J.M. Weiss, C. Allen, R. Shivakumar, S. Feller, L.H. Li, L.N. Liu, Efficient responses in a murine renal tumor model by electroloading dendritic cells with whole-tumor lysate, J. Immunother. 28 (2005) 542–550.
[12] M. Fechheimer, J.F. Boylan, S. Parker, J.E. Sisken, G.L. Patel, S.G. Zimmer, Transfection of mammalian cells with plasmid DNA by scrape loading and sonication loading, Proc. Natl. Acad. Sci. U. S. A. 84 (1987) 8463–8467.
[13] M.W. Miller, D.L. Miller, A.A. Brayman, A review of in vitro bioeffects of inertial ultrasonic cavitation from a mechanistic perspective, Ultrasound Med. Biol. 22 (1996) 1131–1154.
[14] M. Joersbo, J. Brunstedt, Protein synthesis stimulated in sonicated sugar beet cells and protoplasts, Ultrasound Med. Biol. 16 (1990) 719–724.
[15] D.L. Miller, S.V. Pislaru, J.E. Greenleaf, Sonoporation: mechanical DNA delivery by ultrasonic cavitation, Somat. Cell Mol. Genet. 27 (2002) 115–134.
[16] H.R. Guzman, A.J. McNamara, D.X. Nguyen, M.R. Prausnitz, Bioeffects caused by changes in acoustic cavitation bubble density and cell concentration: a unified explanation based on cell-to-bubble ratio and blast radius, Ultrasound Med. Biol. 29 (2003) 1211–1222.
[17] W. Wei, B. Zheng-zhong, W. Yong-jie, Z. Qing-wu, M. Ya-lin, Bioeffects of low-frequency ultrasonic gene delivery and safety on cell membrane permeability control, J. Ultrasound Med. 23 (2004) 1569–1582.
[18] H.J. Kim, J.F. Greenleaf, R.R. Kinnick, J.T. Bronk, M.E. Bolander, Ultrasound-mediated transfection of mammalian cells, Hum. Gene Ther. 7 (1996) 1339–1346.
[19] D.B. Tata, F. Dunn, D.J. Tindall, Selective clinical ultrasound signals mediate differential gene transfer and expression in two human prostate cancer cell lines: LnCap and PC-3, Biochem. Biophys. Res. Commun. 234 (1997) 64–67.
[20] M. Duvshani-Eshet, M. Machluf, Therapeutic ultrasound optimization for gene delivery: a key factor achieving nuclear DNA localization, J. Control. Release 108 (2005) 513–528.
[21] W.J. Greenleaf, M.E. Bolander, G. Sarkar, M.B. Goldring, J.F. Greenleaf, Artificial cavitation nuclei significantly enhance acoustically induced cell transfection, Ultrasound Med. Biol. 24 (1998) 587–595.
[22] Y. Taniyama, K. Tachibana, K. Hiraoka, M. Aoki, S. Yamamoto, K. Matsumoto, T. Nakamura, T. Ogihara, Y. Kaneda, R. Morishita, Development of safe and efficient novel nonviral gene transfer using ultrasound: enhancement of transfection efficiency of naked plasmid DNA in skeletal muscle, Gene Ther. 9 (2002) 372–380.
[23] S. Chen, J.H. Ding, R. Bekeredjian, B.Z. Yang, R.V. Shohet, S.A. Johnston, H.E. Hohmeier, C.B. Newgard, P.A. Grayburn, Efficient gene delivery to pancreatic islets with ultrasonic microbubble destruction technology, Proc. Natl. Acad. Sci. U. S. A. 103 (2006) 8469–8474.
[24] A. Aoi, Y. Watanabe, S. Mori, M. Takahashi, G. Vassaux, T. Kodama, Herpes simplex virus thymidine kinase-mediated suicide gene therapy using nano/microbubbles and ultrasound, Ultrasound Med. Biol. 34 (2008) 425–434.
[25] Z.P. Shen, A.A. Brayman, L. Chen, C.H. Miao, Ultrasound with microbubbles enhances gene expression of plasmid DNA in the liver via intraportal delivery, Gene Ther. (2008).
[26] S. Sonoda, K. Tachibana, E. Uchino, A. Okubo, M. Yamamoto, K. Sakoda, T. Hisatomi, K.H. Sonoda, Y. Negishi, Y. Izumi, S. Takao, T. Sakamoto, Gene transfer to corneal epithelium and keratocytes mediated by ultrasound with microbubbles, Investig. Ophthalmol. Vis. Sci. 47 (2006) 558–564.
[27] K. Iwanaga, K. Tominaga, K. Yamamoto, M. Habu, H. Maeda, S. Akifusa, T. Tsujisawa, T. Okinaga, J. Fukuda, T. Nishihara, Local delivery system of cytotoxic agents to tumors by focused sonoporation, Cancer Gene Ther. 14 (2007) 354–363.
[28] R. Bekeredjian, S. Chen, P.A. Grayburn, R.V. Shohet, Augmentation of cardiac protein delivery using ultrasound targeted microbubble destruction, Ultrasound Med. Biol. 31 (2005) 687–691.
[29] R. Bekeredjian, H.F. Kuecherer, R.D. Kroll, H.A. Katus, S.E. Hardt, Ultrasound-targeted microbubble destruction augments protein delivery into testes, Urology 69 (2007) 386–389.
[30] T. Yamashita, S. Sonoda, R. Suzuki, N. Arimura, K. Tachibana, K. Maruyama, T. Sakamoto, A novel bubble liposome and ultrasound-mediated gene transfer to ocular surface: RC-1 cells in vitro and conjunctiva in vivo, Exp. Eye Res. 85 (2007) 741–748.

[31] R. Suzuki, T. Takizawa, Y. Negishi, K. Hagisawa, K. Tanaka, K. Sawamura, N. Utoguchi, T. Nishioka, K. Maruyama, Gene delivery by combination of novel liposomal bubbles with perfluoropropane and ultrasound, J. Control. Release 117 (2007) 130–136.
[32] R. Suzuki, T. Takizawa, Y. Negishi, N. Utoguchi, K. Maruyama, Effective gene delivery with novel liposomal bubbles and ultrasonic destruction technology, Int. J. Pharm. 354 (2008) 49–55.
[33] R. Suzuki, T. Takizawa, Y. Negishi, N. Utoguchi, K. Sawamura, K. Tanaka, E. Namai, Y. Oda, Y. Matsumura, K. Maruyama, Tumor specific ultrasound enhanced gene transfer in vivo with novel liposomal bubbles, J. Control. Release 125 (2008) 137–144.
[34] R. Suzuki, T. Takizawa, Y. Negishi, N. Utoguchi, K. Maruyama, Effective gene delivery with liposomal bubbles and ultrasound as novel non-viral system, J. Drug Target. 15 (2007) 531–537.
[35] J.D. Pfeifer, M.J. Wick, R.L. Roberts, K. Findlay, S.J. Normark, C.V. Harding, Phagocytic processing of bacterial antigens for class I MHC presentation to T cells, Nature 361 (1993) 359–362.
[36] K. Inaba, M. Inaba, M. Deguchi, K. Hagi, R. Yasumizu, S. Ikehara, S. Muramatsu, R.M. Steinman, Granulocytes, macrophages, and dendritic cells arise from a common major histocompatibility complex class II-negative progenitor in mouse bone marrow, Proc. Natl. Acad. Sci. U. S. A. 90 (1993) 3038–3042.
[37] D.P. Guo, X.Y. Li, P. Sun, Y.B. Tang, X.Y. Chen, Q. Chen, L.M. Fan, B. Zang, L.Z. Shao, X.R. Li, Ultrasound-targeted microbubble destruction improves the low density lipoprotein receptor gene expression in HepG2 cells, Biochem. Biophys. Res. Commun. 343 (2006) 470–474.
[38] T. Mosmann, Rapid colorimetric assay for cellular growth and survival: application to proliferation and cytotoxicity assays, J. Immunol. Methods 65 (1983) 55–63.
[39] S.E. Slezak, P.K. Horan, Cell-mediated cytotoxicity. A highly sensitive and informative flow cytometric assay, J. Immunol. Methods 117 (1989) 205–214.
[40] G. Reinhard, A. Marten, S.M. Kiske, F. Feil, T. Bieber, I.G. Schmidt-Wolf, Generation of dendritic cell-based vaccines for cancer therapy, Br. J. Cancer 86 (2002) 1529–1533.
[41] M. Kinoshita, K. Hynynen, Intracellular delivery of Bak BH3 peptide by microbubble-enhanced ultrasound, Pharm. Res. 22 (2005) 716–720.
[42] I.V. Larina, B.M. Evers, R.O. Esenaliev, Optimal drug and gene delivery in cancer cells by ultrasound-induced cavitation, Anticancer Res. 25 (2005) 149–156.
[43] M. Duvshani-Eshet, D. Adam, M. Machluf, The effects of albumin-coated microbubbles in DNA delivery mediated by therapeutic ultrasound, J. Control. Release 112 (2006) 156–166.
[44] C.M. Newman, T. Bettinger, Gene therapy progress and prospects: ultrasound for gene transfer, Gene Ther. 14 (2007) 465–475.
[45] R.K. Schlicher, H. Radhakrishna, T.P. Tolentino, R.P. Apkarian, V. Zarnitsyn, M.R. Prausnitz, Mechanism of intracellular delivery by acoustic cavitation, Ultrasound Med. Biol. 32 (2006) 915–924.
[46] P.M. Kloetzel, Antigen processing by the proteasome, Nat. Rev. Mol. Cell. Biol. 2 (2001) 179–187.

J Med Ultrasonics (2008) 35:5–10
DOI 10.1007/s10396-007-0163-x

ORIGINAL ARTICLE

Taira ZENITANI · Ryo SUZUKI · Kazuo MARUYAMA
Hiroshi FURUHATA

Accelerating effects of ultrasonic thrombolysis with bubble liposomes

Received: May 23, 2007 / Accepted: September 28, 2007

Abstract
Purpose. The accelerating effect on thrombolysis by combined use of 500-kHz low-frequency ultrasound (US), recombinant tissue plasminogen activator (rt-PA), and bubble liposomes (BLs) was verified in vitro.
Methods. A fibrin clot was formed by adding thrombin to bovine plasma. It was enclosed in a pressurized container, the pressure and temperature of which were maintained at 150 mmHg and 37°C, respectively. Ultrasonic conditions were set at a continuous wave, a frequency of 500 kHz, an intensity of 0.7 W/cm^2, and a sonication time of 60 s. We derived the rate of reduction in clot weight from the decreased clot weight and the weight before sonication. We compared the rate of reduction in groups combining physiological saline, rt-PA, BLs, and US.
Results. Only the rt-PA+US+BL group showed a significantly accelerated thrombolytic effect compared with any other group or with any combination of two factors in the 60-s period ($0.001 < P < 0.027$).
Conclusion. BLs have great potential to accelerate the thrombolytic effect of rt-PA with low-frequency, 500-kHz, continuous-wave ultrasound.

Keywords ultrasound · thrombolysis · bubble · liposome

Introduction

As clot recanalization therapy for acute myocardial infarct and more recently for acute cerebral infarct, a thrombolytic agent with a high affinity for clots, i.e., recombinant tissue plasminogen activator (rt-PA), is intravenously administered.[1,2] For all acute ischemic conditions, the sooner blood flow recanalization is achieved, the better the outcome. Hence, as a measure to enhance the thrombolytic effect of rt-PA, the combined use of ultrasound (US) was developed with limited application in clinical practice. It has been shown that monitoring with diagnostic transcranial Doppler (TCD) ultrasound (US) at 2 MHz with rt-PA treatment increases the recanalization rate 2 h after the procedure in most acute ischemic stroke cases in which urgent ischemic recanalization is indicated.[3] On the other hand, although still at the in vitro/in vivo experimental stage, a study showed that for ultrasonography in the range of some tens of kilohertz, i.e., lower than the diagnostic megahertz range, 1 h of radiation-accelerated thrombolysis yielded higher thrombolytic rates than the diagnostic US range did.[4] However, the outcome was neurologically evaluated at 3 months and improvement was still seen in only 20%–30% of cases.

As a technology to further improve the thrombolysis-enhancing effects of this US treatment, the efficacy of microbubbles (MBs), a US contrast medium, has also been demonstrated clinically. A study showed that with rt-PA administration, if additional contrast medium was administered to acute cerebral infarct patients during TCD monitoring, the complete recanalization rate 2 h after the procedure was 40.8% for those co-administered rt-PA and TCD, whereas adding MBs increased the rate significantly to 54.5%.[5]

For the latest treatment currently given to patients with ischemic disease, i.e., a combination of thrombolytic agents, US, and MBs, the recanalization time is not yet clinically satisfactory. In dealing with these problems, in terms of the US conditions and MBs, the following technical challenges remain. As to the US conditions, instead of the diagnostic wavelength range, utilization of the range between some tens and some hundreds of kilohertz, for which efficacy has not been well documented in either in vitro or in vivo studies, may be considered.[6–8] Improvement in thrombolytic recanalization rates and shortening of the recanalization time are anticipated in the clinical setting with low-frequency, low-intensity US. Moreover, enhanced efficacy by employing additional MBs may be associated with clot

T. Zenitani (✉) · H. Furuhata
Medical Engineering Laboratory, Research Center for Medical Science, Jikei University School of Medicine, 3-25-8 Nishishinbashi, Minato-ku, Tokyo 105-8461, Japan
Tel. +81-3-3433-1111; Fax +81-3-3459-6005
e-mail: taira_z@jikei.ac.jp

R. Suzuki · K. Maruyama
Department of Biopharmaceutics, School of Pharmaceutical Sciences, Teikyo University, Tsukui, Japan

surface invasion by bubble breakthrough. Currently, a variety of imaging media are commercially available, but their bubbles are several micrometers in diameter, and no studies have examined the efficacy of applying bubbles with a diameter of several hundreds of nanometers, which are highly likely to penetrate clots.

This study, in an effort to achieve shorter thrombolysis times, employed a 500-kHz continuous wave (CW) US, which one of the present authors had been examining for US conditions,[7] because this is the only condition for which the efficacy and safety of the TCD method have been shown in animal experiments. We employed perfluoropropane (PFP)-enclosed bubbles, i.e., novel bubble liposomes (BLs) based on the liposomes prepared by Suzuki et al.[9,10] Because these BLs contain bubbles with a diameter of several hundreds of nanometers, they may pass through 5-μm fibrin nets, thereby invading clots more effectively. For evaluation of the thrombolytic time-shortening effect in particular, we conducted an in vitro study of rt-PA, US, and BLs to assess clot weight loss rates at 1 min after application. Since the effects of a conventional combination of rt-PA and US are reportedly expressed approximately 5 min after application,[11] we compared the efficacy in as little as one-fifth of this time to clarify the efficacy of a shorter time period.

Subjects and methods

Preparation of BLs

We prepared BLs in accordance with the method proposed by Suzuki et al.[9,10] First, 2 ml of liposome solution (NOF, Japan) (lipid content 1 mg/ml) and 5 ml of PFP (Takachiho, Japan) were placed in a 5-ml vial that was then tightly closed. Another 7.5 ml of PFP was added and then irradiated with 42-kHz US in an ultrasonic cleaner (2510J-DTH, Branson Ultrasonics/Emerson Japan, Japan) to prepare the BLs. The almost clear liposome solution became cloudy as a result of this procedure. The particle size distributions of these BLs and liposome solution were measured using a dynamic light-scattering particle size distribution meter (Zetasizer, Sysmex). At the same time, we observed BLs using a light microscope (Eclipse 80i, NIKON) and a digital finescope (VC7700, Omron).

Measurement of BL elimination rate and determination of acoustic intensity

Figure 1a depicts BLs before US radiation and Fig. 1b shows BLs after US radiation. Clear cellophane was spread on the bottom of each cylindrical acrylic tube with an inside diameter of 1 cm, and 1 ml of BL solution was infused. The US used was a CW generated by a circular Lead Titanate Ziroonate transducer (Φ 10 mm) (Honda Electronics, Japan) at 500 kHz and an acoustic intensity of 0.7 W/cm^2 spatial peak temporal average (SPTA). The exposure time was 60 s (amplifier, high-speed power amplifier 4055, NF, Japan; signal generator, Wave factory 1941, NF). From the bottom of this cylinder, US radiation was used to measure the mean luminance of BLs in the central part of the container (Fig. 1, central circle) before and after exposure to US radiation. The postradiation value was subtracted from the preradiation value and then divided by the preradiation value to determine the BL elimination rate (this technique is hereinafter referred to as the scattering light simplified measurement method). For different levels of the acoustic intensity, each cylinder was measured five times to determine the mean value. The best acoustic intensity was thus determined to be 0.7 W/cm^2, based on the acoustic intensity versus BL elimination curve, and this level was employed in the study.

Verification of the thrombolysis effect

In this study, we used a fibrin clot prepared by treating bovine plasma (Sigma-Aldrich, Japan) with 20 μl of thrombin (100 IU/ml) (Sigma-Aldrich). In order to minimize the contact area, the clot was encapsulated in a pressurized container using a pincette with a thin diffracted tip (Suncraft, Japan) to prevent the fibrin clot from breaking. Then, while measuring the pressure in the container using a manometer (DG-100-102GP, Copal Electronics, Japan), it was gradually pressurized with a 5-ml syringe to 150 mmHg

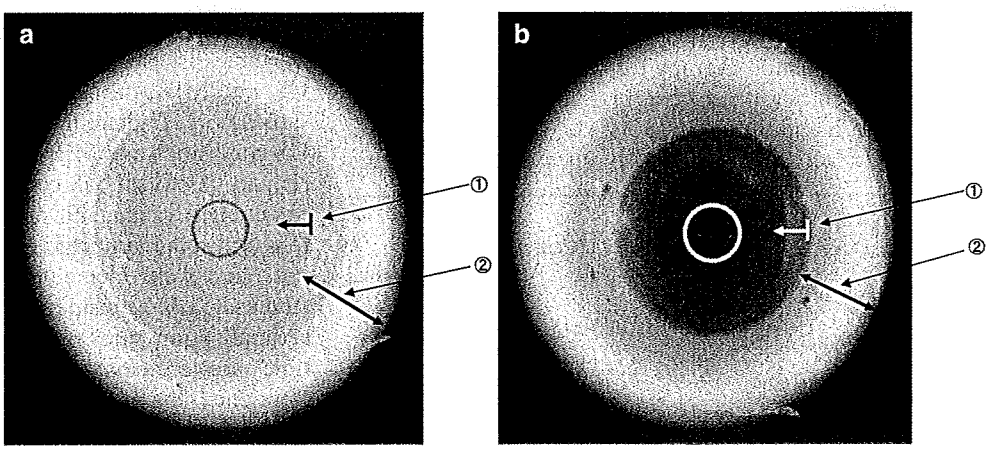

Fig. 1a,b. Changes in the luminosity of a bubble liposome (BL) solution. The average luminosity in the *circle* was measured: **a** BLs before sonication and **b** BLs after sonication [continuous wave (CW), 500 kHz, 0.7 W/cm^2, 60 s]. *1*, BLs; *2*, acrylic tube

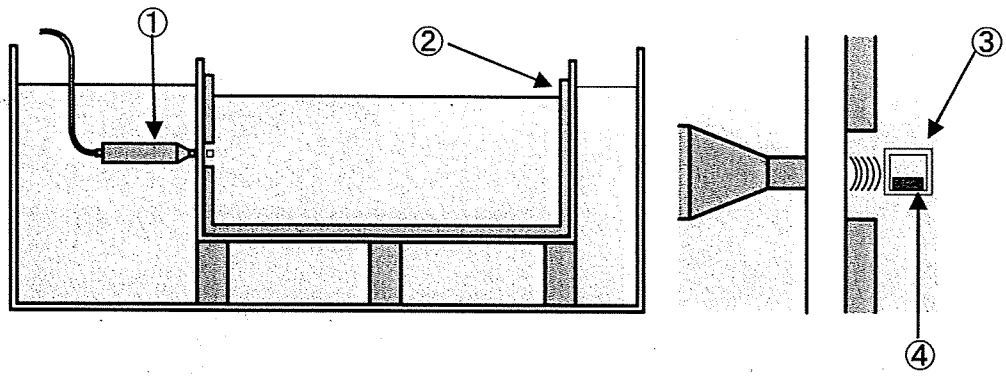

Fig. 2. Experimental system for sonication: *1*, 500-kHz transducer; *2*, sound-absorbing foam; *3*, container; *4*, fibrin clot

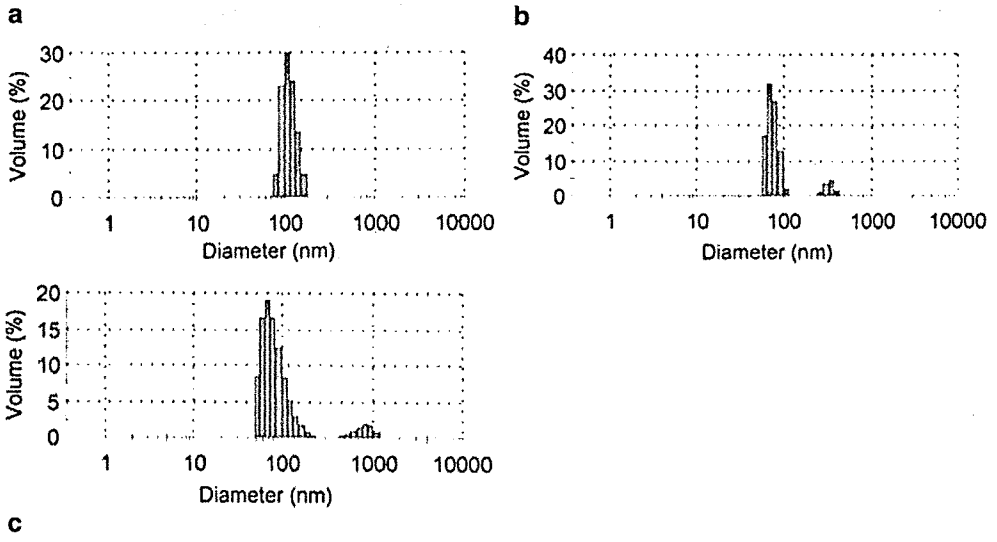

Fig. 3. Size distribution by dynamic light scattering. **a** Liposomes measured within 2 min of shaking are mostly 120 nm in diameter. **b** BLs measured within 2 min of shaking: 50–100 nm and 200–400 nm. **c** BLs measured from 2 to 4 min after shaking: 50–200 nm and 1 μm or more

and 37°C. Then, US radiation was applied using the setup shown in Fig. 2. The thrombolytic effect was evaluated by the fibrin clot weight loss rates. Because the fibrin clot should be weighed after the elimination of water content around the clot, the fibrin clot was placed on a 50-μm mesh (PET51-HC, Tanaka Sanjiro, Japan), and the water filtering through the mesh was absorbed with absorbent paper (Kimwipe Wiper S-200, Nippon Paper Crecia, Japan) for measurement with an analytical balance (AB104-S, Mettler Toledo, Switzerland) (minimum indication: 0.1 mg). Without directly touching the clot so as to avoid losing water contained in the fibrin clot, we simply replaced the absorbent paper placed under the mesh. The weight loss rates were determined as (pre-encapsulation weight – post-US radiation weight)/pre-encapsulation weight. The time from fibrin clot encapsulation to measurement of post-US radiation weight was set at 3 min. The US conditions were set as determined above, i.e., CW, 500 kHz, 0.7 W/cm^2 (SPTA), and 60 s. The acoustic intensity was measured in a nonpressurized container using a needle-type hydrophone (HNC-0400, ONDA, CA, USA). We used the following four types of solutions: physiological saline (control group), physiological saline solution prepared with BLs at 0.5 mg/ml (BL group), physiological saline solution prepared with rt-PA (monteplase) at 1000 IU/ml (rt-PA group), and physiological saline solution prepared with rt-PA at 1000 IU/ml and BLs at 0.5 mg/ml (rt-PA + BL group).

Evaluation method

We compared groups using the *t* test to confirm that there were no differences in pre-US radiation fibrin clot weight between any of the groups. Then, for the control, rt-PA, BL, and rt-PA + BL groups with and without US radiation, i.e., a total of eight groups (control, rt-PA, BL, rt-PA + BL, US, rt-PA + US, BL + US, and rt-PA + BL + US groups), ten clots per group were statistically compared using the *t* test.

Results

BL particle size distribution

The particle size distribution of liposomes and BLs determined by the dynamic light scattering method are presented in Figs. 3a–c. Fig. 3a presents the particle size distribution of the liposomes, showing a central diameter of approximately 120 nm and a distribution range of 70–200 nm. Figures 3b and 3c present the analytical results for the BL particle distribution at 0–2 min and 2–4 min after shaking by hand, respectively. The distributions in the two groups were between 50 and 100 nm and between 200 and 400 nm at 0–2 min. At 2–4 min, the distribution range widened and was divided into one group at 50–200 nm and another at more

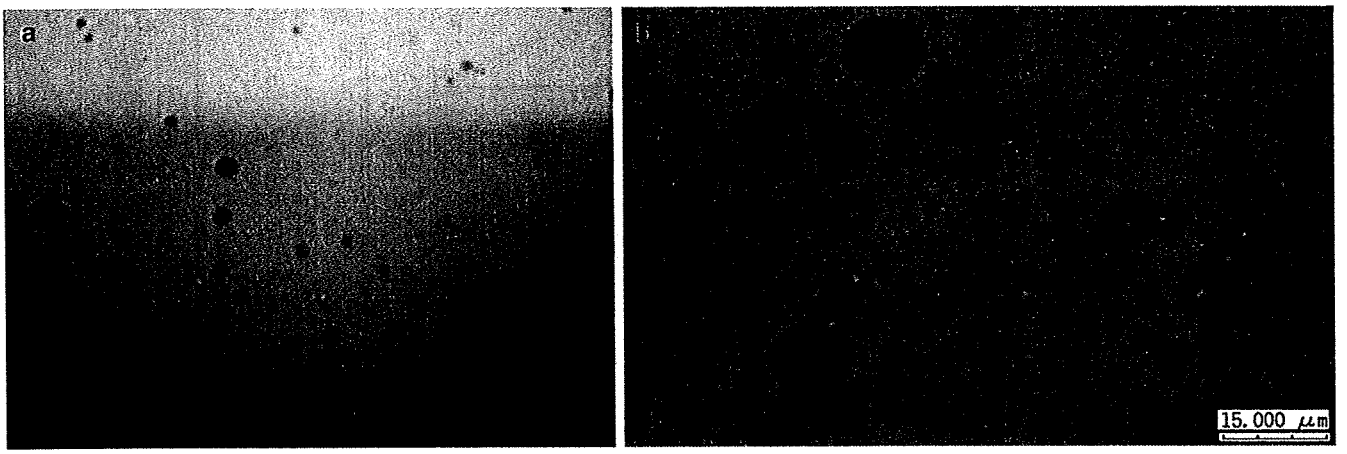

Fig. 4a,b. Photomicrographs of BLs. **a** Light microscopic view (×400) and **b** digital finescope view (×7000)

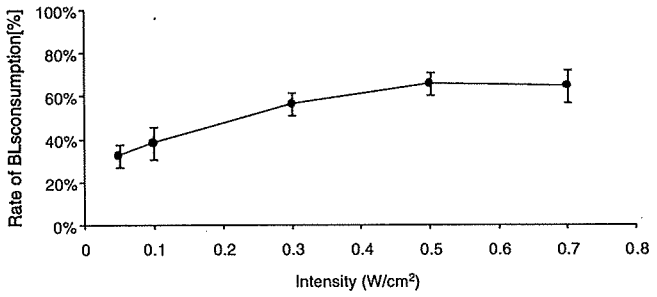

Fig. 5. Relation between ultrasound (US) intensity (CW, 500 kHz, 60 s) and rate of BL consumption: 62% at the maximum intensity 0.5 W/cm^2 ($n = 3$)

than 1 μm. This may be because the BL concentration fluctuates within the observation range of 100 μm, and the distribution changes with time. This phenomenon is shown in Figs. 3b and 3c.

Observations made with a light microscope and a digital finescope are presented in Figs. 4a and 4b, respectively. The prepared BLs were observed to vary in size and to change over time. There were some micro-orders not measurable with the dynamic light scattering method.

Occurrence of microcavitation

Figure 5 shows the BL elimination rate for various levels of acoustic intensity using the scattering light simplified measurement method. The higher the acoustic intensity, the higher the BL elimination rate, and when the intensity exceeded approximately 0.5 W/cm^2, the elimination rate showed a roughly constant value. From these results, the acoustic intensity for the experiments was set at 0.7 W/cm^2. This acoustic intensity was determined under nonpressurized conditions.

Weight reduction rate

Figure 6a shows a prepared fibrin clot. The photograph was taken with the fibrin clot placed on a 50-μm mesh. The elastic, yellowish-white, cylindrical fibrin clots were encapsulated in a pressurized container and radiated with US. Figure 6b shows the fibrin clot after US radiation; the size was clearly reduced.

Figure 7 shows that there were no differences in fibrin clot weight among the groups before US radiation. Figure 8 shows the weight reduction rates for fibrin clots in each solution with or without US radiation. Comparisons among the control, BL, and BL + US groups revealed the mean clot weight reduction rate and variances to be 24.2 ± 3.6%, 24.9 ± 4.8%, and 25.8 ± 3.2%, respectively, and when BLs were administrated alone or with US radiation (500 kHz), no enhancement of thrombolysis was observed (P>0.05). A comparison between the control and rt-PA groups revealed weight reduction rates of 24.2 ± 3.6% and 24.2 ± 2.8%, respectively, with no significant difference (P = 0.30), and exposure to US did not enhance the thrombolytic effect of rt-PA. There were no differences in individual single-drug effects or weights in relation to the two active elements.

However, compared with the other seven groups, the rt-PA + BL + US group exhibited a significantly increased weight reduction (29.2 ± 3.0%, 0.001 < P < 0.027). There were no significant differences among the other two groups except for the rt-PA + BL + US group (0.25 < P < 0.99). Based on these results, the significant enhancement of thrombolytic rate observed for the rt-PA + BL + US group was the result of the three overlapping effects of the individual treatments.

Discussion

In this study, a combination of rt-PA, BLs, and US increased the thrombolytic rate of bovine fibrin clots after 1 min. To date, studies have reported the enhancement of thrombolysis with MBs, but herein it was shown that BLs may accelerate thrombolysis when applied with rt-PA and US.

Siegel et al. reported that a combination of perfluorocarbon-exposed sonicated dextrose albumin (PESDA) and percutaneous US radiation (37 kHz, 160 W max., 60 min) resulted in 100% recanalization in a rabbit clot infarction

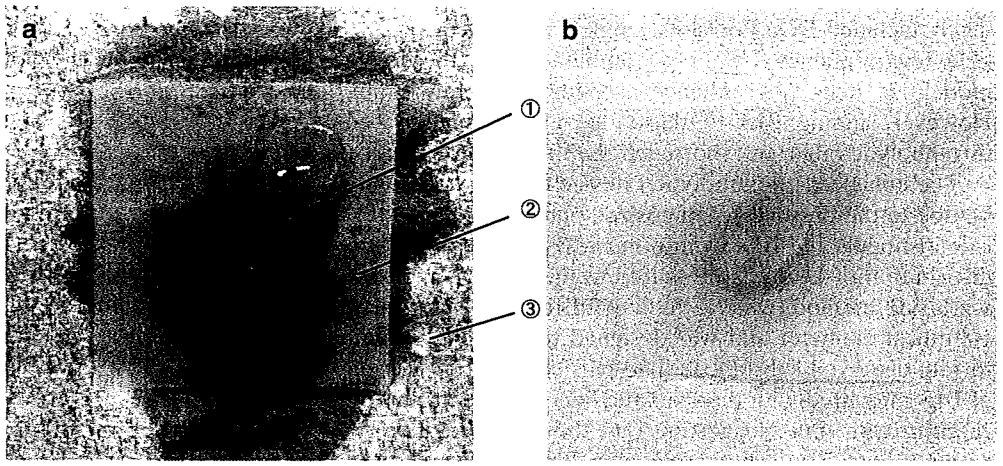

Fig. 6. A fibrin clot **a** before sonication (*1*, fibrin clot; *2*, 50-μm mesh; *3*, absorption paper) and **b** after sonication

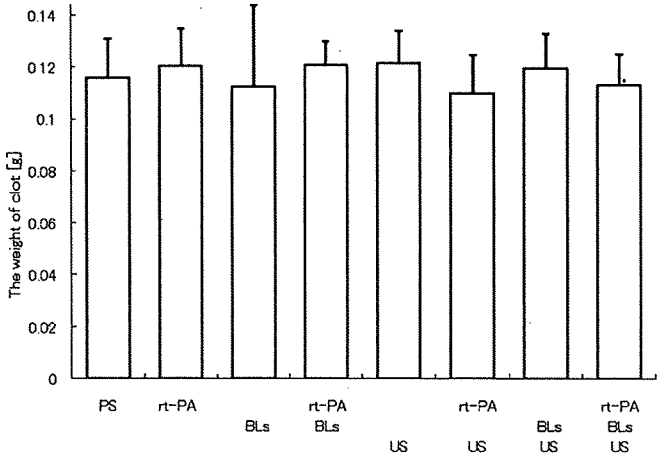

Fig. 7. Weight of clots before sonication. There were no differences in the clot weights before sonication among the groups. Data are expressed as mean ± SD (n = 10). *PS*, physiological saline; *rt-PA*, recombinant tissue plasminogen activator

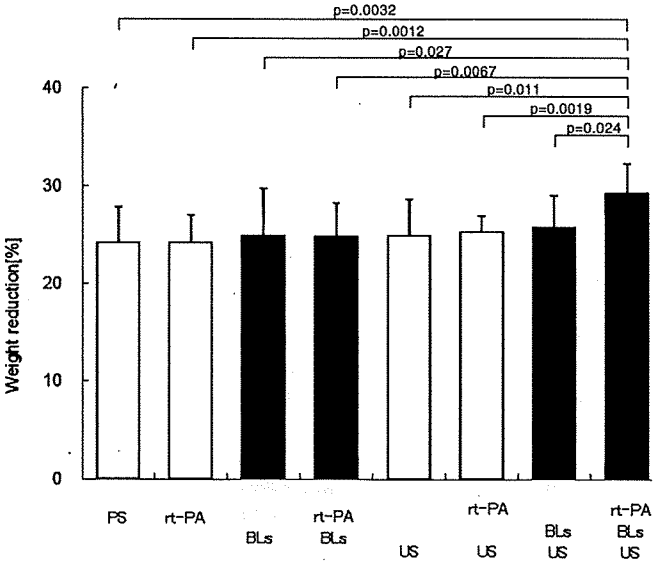

Fig. 8. Comparison of the rates of decrease in fibrin clot weight under various treatments: rt-PA (monteplase 1000 IU/ml), BLs (lipid 0.5 mg/ml), US (CW, 500 kHz, 60 s). Compared with any other group or with any combination of two factors, the clot weight reduction was significantly larger for the rt-PA+BL+US group ($P < 0.05$). Data are expressed as mean ± SD (n = 10)

model.[12] They employed US at approximately one-tenth of the frequency used in our experiments, and the mechanical index (MI) was about 3.3 times greater (MI is actually defined by the pulse wave, and so MI is not directly applicable to CW, or a burst wave, but there is no other appropriate index, and MI was thus applied). Although our BLs had a lower MI than those of Siegel et al, adding rt-PA enhanced the thrombolytic rate obtained at 1 min.

Mizushige et al. also showed that a combination of rt-PA and US radiation (CW, 10 MHz, 1.02 W/cm^2, 10 min) in addition to MBs [dodecafluoropentane (DDFP)] yielded a clot weight reduction rate of 49% in an in vitro study of human white thrombi.[13] Compared with their experimental conditions, our frequency was 1/20 and the exposure time was 1/10, and because of clot variations we cannot compare our results with theirs directly, but we did compare the weight reduction rates: 29% for the rt-PA + BL + US group versus 49%. The superimposed effects of the three elements, rt-PA, BLs, and US, may increase thrombolytic rates even at 10 min after administration; such temporal changes will be examined further.

Spengos et al. conducted a study evaluating temporal increases in thrombolytic rates using a flow model.[11] The starting point of increases in recanalization flow was 15 min for use of rt-PA alone, but this was shortened to 5 min with the combination of rt-PA and 1-MHz US exposure, and increased thrombolytic rates were observed when rt-PA was enhanced by US. However, even though they used the same bovine fibrin clot that we did, no enhanced recanalization flow was observed at 1 min after application. We did not evaluate such temporal changes but we did show that within 1 min, while no thrombolytic effect was observed in their study, the superimposed effects of the three elements, including BLs, enhanced the thrombolytic rates in our model.

The achievement of enhanced thrombolytic rates in as short a time as 1 min may be largely attributable to the

newly included BLs. For clots, single use of rt-PA or 500-kHz low-frequency US or a combination of these two modalities does not enhance thrombolysis after 1 min. However, adding BLs to these two elements enhanced thrombolytic rates, i.e., shortened the thrombolysis time.

The enhanced thrombolytic rates achieved by BLs may be due to the presence of nanosized particles, a characteristic distinguishing BLs from other MBs. The particle size distribution of BLs was measured using the dynamic light scattering method, which was limited to a detection area 100 μm in diameter and was designed to be used for uniformly dissolved substances. The particle size distribution of BLs measured with the dynamic light scattering method changed with time, suggesting that the delicate condition within the small detection range may fluctuate on an hourly basis. It was suggested that BLs might contain very small bubbles of approximately 120 nm in diameter and larger bubbles with diameters of 1–2 μm. However, cumulative formation of microsized air bubbles via aggregation of very small air bubbles of about 100 μm in diameter should also perhaps be considered. We prepared BLs using the same technique as that of Suzuki et al., though their BLs were approximately 3 μm in size, whereas ours contained massive bubbles. We will conduct further studies to ascertain why this difference in bubble size distribution occurred. In addition, we will also compare our bubbles with other bubbles.

Because the pore space of the fibrin net in clots is approximately 5 μm,[14] BLs containing nanosized particles in addition to microsized particles may pass through these pores. However, as clarified by the experiments, even though BLs alone permeated the fibrin net, no enhancement of the thrombolytic rate was observed.

Francis et al. proposed that 1-MHz, 4-W/cm^2 US radiation reversibly extended the fibrin structure, facilitating rt-PA penetration.[15] However, the present experiment employed US conditions different from those in their report, and because of the one-half frequency and one-sixth acoustic intensity used herein, only slight fibrin structure extension may have occurred.

Tachibana, using electron micrography, reported how microjets generated on the elimination of MBs were hitting cell surfaces.[16] Even in the absence of an extended fibrin structure due to this physical phenomenon, microjets generated around the fibrin clot by cavitation may have enhanced infiltration of BLs and rt-PA into the fibrin clot.

As a result, the superimposed effects of the three elements (BLs containing submicrosized particles, US-generated microjets and microvibration, and rt-PA) appear to have yielded enhanced clot thrombolytic rates.

The present study used thrombin–fibrin clots. In clinical practice, we see atherothrombosis and platelet thrombus in addition to thrombin clots, and whether results similar to those described here would be obtained with these clots is unknown. The efficacy against these types of clots needs to be examined further.

Conclusion

We confirmed that bubble liposomes with rt-PA and low-frequency US increased thrombolytic rates even in a very short time, i.e., in as little as 1 min.

References

1. The GUSTO investigators. An international randomized trial comparing four thrombolytic ratagies for actice myocardial infarction. The GUSTO investigators. N Engl J Med 1993;329(10):673–82.
2. The National Institute of Neurological Disorders and Stroke rt-PA Stroke Study Group. Tissue plasminogen activator for acute ischemic stroke. N Engl J Med 1995;333:1581–7.
3. Alexandrov AV, Molina CA, Grotta Z, et al. Ultrasound-enhanced systemic thrombolysis for acute ischemic stroke. N Engl J Med 2004;351:2170–8.
4. Suchkova V, Siddiqi FN, Carstensen EL, et al. Enhancement of fibrinolysis with 40-kHz ultrasound. Circulation 1998;98:1030–5.
5. Molina CA, Ribo M, Rubiera M, et al. Microbubble administration accelerates clot lysis during continuous 2-MHz ultrasound monitoring in stroke patients treated with intravenous tissue plasminogen activator. Stroke 2006;37(2):425–9.
6. Behrens S, Daffertshofer M, Spiegel D, et al. Low-frequency, low-intensity ultrasound accelerates thrombolysis through the skull. Ultrasound Med Biol 1999;25(2):269–73.
7. Ishibashi T, Akiyama M, Onoue H, et al. Can transcranial ultrasonication increase recanalization flow with tissue plasminogen activator? Stroke 2002;33:1399–1404.
8. Tachibana K, Tachibana S. Albumin microbubble echo-contrast material as an enhancer for ultrasound-accelerated thrombolysis. Circulation 1995;92(5):1148–50.
9. Suzuki R, Takizawa T, Negishi Y, et al. Gene delivery by combination of novel liposomal bubbles with perfluoropropane and ultrasound. J Controlled Release 2007;117(1):130–6.
10. Suzuki R, Takizawa T, Negishi Y, et al. Tumor-specific ultrasound-enhanced gene transfer in vivo with novel liposomal bubbles. J Controlled Release 2008;125(2):137–44.
11. Spengos K, Behrens S, Daffertshofer M, et al. Acceleration of thrombolysis with ultrasound through the cranium in a flow model. Ultrasound Med Biol 2000;26(5):889–95.
12. Siegel RJ, Atar S, Fishbein MC, et al. Noninvasive transcutaneous low-frequency ultrasound enhances thrombolysis in peripheral and coronary arteries. Echocardiography 2001;18(3):247–57.
13. Mizushige K, Kondo I, et al. Enhancement of ultrasound-accelerated thrombolysis by echo contrast agents: dependence on microbubble structure. Ultrasound Med Biol 1999;25(9):1431–7.
14. Carr ME Jr, Hardin CL. Fibrin has larger pores when formed in the presence of erythrocytes. Am J Physiol 1987;253(5 Pt 2): H1069–73.
15. Francis CW, Blinc A, Lee S, et al. Ultrasound accelerates transport of recombinant tissue plasminogen activator into clots. Ultrasound Med Biol 1995;21(3):419–24.
16. Tachibana K. Application of microbubbles for therapy. Med Biol Eng 2005;43(2):211–5.

Biochemical and Biophysical Research Communications 377 (2008) 1062–1066

Contents lists available at ScienceDirect

Biochemical and Biophysical Research Communications

journal homepage: www.elsevier.com/locate/ybbrc

Nuclear localization of SNARK; its impact on gene expression

Wataru Kuga [a,b], Katsuya Tsuchihara [b], Tsutomu Ogura [c], Sakyo Kanehara [a,b], Marie Saito [a,b], Atsushi Suzuki [d], Hiroyasu Esumi [a,b,*]

[a] Department of Integrated Biosciences, Graduate School of Frontier Sciences, The University of Tokyo, Kashiwa, Chiba 277-8561, Japan
[b] Cancer Physiology Project, Research Center for Innovative Oncology, National Cancer Center Hospital East, Kashiwa, Chiba 277-8577, Japan
[c] Department of Bioinformatics Sciences, Faculty of Pharmaceutical Sciences, Hokuriku University, Kanazawa, Ishikawa 920-1180, Japan
[d] Division of Endocrinology and Metabolism, Department of Developmental Physiology, National Institute for Physiological Sciences, Okazaki, Aichi 444-8585, Japan

ARTICLE INFO

Article history:
Received 10 October 2008
Available online 6 November 2008

Keywords:
SNARK
AMPK-related kinase
Nuclear localization signal
Transcriptome

ABSTRACT

SNARK, a member of the AMPK-related kinases, has been involved in the cellular stress responses but its precise mechanisms remain unclear. Subcellular localization of SNARK protein was identified. Unlike cytoplasmic localizing AMPKα, SNARK was predominantly localized in the nucleus. SNARK was constitutively distributed in the nucleus even when SNARK was activated by metabolic stimuli such as AICAR and glucose-deprivation. Conserved nuclear localization signal (NLS) was identified at the N-terminal portion (^{68}KKAR^{71}). Deletion and point mutation of this part resulted in the cytoplasmic translocation of mutant proteins. Furthermore, GFP fused with the SNARK fragment containing ^{68}KKAR^{71} translocated to the nucleus. A microarray analysis revealed that the nuclear localizing SNARK altered transcriptome profiles and a considerable part of these alterations were canceled by the mutation of NLS, suggesting the ability of SNARK to modulate gene expression dependent on its nuclear localization.

Introduction

AMPK (AMP-activated protein kinase) is a well-known cellular energy sensor. AMPK is activated in response to various metabolic stresses [1]. Once activated, AMPK phosphorylates a variety of substrates to increase catabolic pathways and decrease anabolic pathways, resulting in the maintenance of cellular energy balance [2]. AMPK is a heterotrimeric enzyme composed of an α-catalytic subunit, and β- and γ-regulatory subunits [3,4]. Two isoforms of the α-subunit have been identified. AMPKα1 constitutively resides in the cytoplasm, whereas a portion, but not all, of the activated α2-subunit translocates to the nucleus [5–8].

Human kinome information predicted that 12 kinases are closely related to AMPK [9,10]. SNARK (SNF1/AMPK-related kinase, also known as NUAK2) is a member of the AMPK-related kinases [11]. SNARK was originally isolated as an ultraviolet B (UVB)-induced gene in rat karatinocytes. Similar to AMPK, the kinase activity of SNARK is up-regulated by metabolic stresses [12]. Furthermore, *Snark*-deficient mice exhibited mature-onset obesity and related metabolic disorders [13]. These findings suggest the potential relevance of SNARK in cellular responses against metabolic stresses.

In this study, we attempted to identify the subcellular localization of SNARK. We found that SNARK was consistently localized in the nucleus. We also found that SNARK was activated by AICAR as well as glucose-deprivation. We further identified the responsible nuclear localization signal (NLS) of SNARK. Finally, transcriptome profiles of wild-type and NLS mutant SNARK expressing cells were compared to identify the impact of the nuclear localization of SNARK upon the regulation of mRNA levels of potential downstream genes.

Materials and methods

Plasmid construction. The FLAG-tagged SNARK protein-expressing plasmid vector, pFLAG-SNARK has been described elsewhere[14]. pFLAG-SNARK-(2-447) was constructed by PCR amplification of the DNA sequences coding FLAG-tag and 2–447 amino acid sequences of SNARK using pFLAG-SNARK as a template and primers containing a 5′ EcoRI site (SNK-D1-F) and a 3′ XhoI site (SNK-D2-R). The PCR product was digested with EcoRI and XhoI and was cloned into pcDNA3.1(−) (Invitrogen). Other deletion mutant-expressing vectors were constructed as well. The PCR primers used to amplify the SNARK fragment were as follows: SNK-D1-F and SNK-D1-R for pFLAG-SNARK-(2–370), SNK-D1-F and SNK-CD(−)-R for pFLAG-SNARK-(2–169), SNK-D2-F and SNK-D2-R for pFLAG-SNARK-(78–447), SNK-CD(−)-F and SNK-D3-R for pFLAG-SNARK-(311–628), and SNK-D3-F and SNK-D3-R for pFLAG-SNARK-(390–628). pSNARK-(1–169)-GFP was constructed by PCR amplification of the 1–169 amino acid coding sequence of SNARK using primers containing a 5′ SacII site (NLS-GFP-F3) and a 3′ NheI

* Corresponding author. Address: Cancer Physiology Project, Research Center for Innovative Oncology, National Cancer Center Hospital East, Kashiwa, Chiba 277-8577, Japan. Fax: +81 4 7134 8676.
E-mail address: hesumi@east.ncc.go.jp (H. Esumi).

0006-291X/$ - see front matter © 2008 Elsevier Inc. All rights reserved.
doi:10.1016/j.bbrc.2008.10.143

site (NLS-GFP-R3). The PCR product was digested with both enzymes and was cloned into pQBI25 (MP Biomedicals, Irvine, CA). Point mutant (^{68}AAAR^{71}) was also generated using two-step PCR. ^{68}AAAR^{71} was constructed using primers SNK-KKAR-F2 and SNK-KKAR-R2 as the internal primers. 3xF-EcoRI and 3xF-XbaI were used as the secondary 5′- and 3′-primers for all point mutants. The resulting amplified products were subcloned into p3xFLAG-CMV (Sigma). Mutated DNA was sequenced over their full-length to verify that they carried only the intended mutation using 3100 Sequencing Analyzer (Applied Biosystems). All the PCR primers used above are provided as Supplementary Table 1.

Cell culture. HeLa and PLC/PRF/5 cells were purchased from the American Tissue Culture Collection and were maintained in Dulbecco's modified Eagle's medium (DMEM, GIBCO) supplemented with 10% fetal bovine serum and antibiotics. Cells were cultured in a humidified chamber at 37 °C in 5% CO_2 in the air.

Transfection and establishment of stable cell lines. Cells were seeded on a 6-well plate at a density of 2×10^5 cells/well and were transfected with 4 μg of plasmid DNA using 10 μl of Lipofectamine2000 (Invitrogen) in 500 μl of Opti-MEM I (Invitrogen) serum-free medium and cultured for 48 h. For the selection of cells stably expressing a neomycin-resistant gene, the cells were transfected with pcDNA3.1-based plasmids and grown for 2 days. Then, 1×10^5 cells were seeded on φ10 cm culture dishes and grown in the medium containing 1000 μg/mL of G418 for 14 days. The G418-containing medium was replaced every 2 days. Individual clones were picked up with incised and sterilized pieces of filter paper and were transferred to 96-well culture plates followed by consecutive transfer to larger culture plates or dishes.

Fluorescent and indirect immunofluorescent microscopy. The cells were seeded on φ35 mm glass-bottomed dishes (Matsunami). For the indirect immunofluorescent microscopy, the cells were fixed in acetone–methanol (1:1) for 10 min at room temperature. The cells were blocked with 2% BSA in PBS for 1 h at room temperature. The cells were incubated with anti-FLAG M2 antibody diluted 1:500 in blocking solution for 1 h at room temperature followed by incubation with anti-mouse Alexa Fluor 488 secondary antibody (Molecular Probes) diluted 1:1000 in blocking solution for 1 h at room temperature. Nuclear DNA was counterstained with PI (Molecular Probes) in blocking solution. The cells were observed using a confocal microscope system (LSM5 PASCAL; ZEISS).

Preparation of cellular extracts. The cells were lysed in SDS lysis buffer (1% SDS, 1 mM Na_3VO_4, 10 mM Tris–HCl, pH 7.4). Nuclear and cytoplasmic extracts were prepared using the NE-PER Kit (Pierce) according to the manufacture's instructions. The protein concentrations were determined using a BCA protein assay kit (Pierce).

Immunoblot assays. Ten micrograms of total proteins was loaded onto a 10% SDS–PAGE and electrophoresed. The separated proteins were transferred to polyvinylidene difluoride membranes (Millipore) using a semi-dry transfer. The membranes were blocked for 2 h at room temperature with 5% nonfat dry milk in PBST buffer (PBS containing 0.1% of Tween 20) and incubated with primary antibody overnight at 4 °C. The membranes were incubated with the secondary antibody conjugated to horseradish peroxidase for 1 h at room temperature. The bands of interest were detected using an ECL chemiluminescence reagent (GE Healthcare). Anti-FLAG M2 and anti-SNARK antibodies were from Sigma, anti-C23 antibody was from Santa Cruz, and anti-HSP90 antibody was from Cell Signaling.

Microarray analysis. PLC/PRF/5 cells were transfected with the empty vector p3xFLAG-CMV, the wild-type SNARK expression vector, or the ^{68}AAAR^{71} expression vector, and incubated for 24 h. Each of total RNA samples was prepared in duplicate. Total RNA was isolated using RNeasy Kit (QIAGEN). Total RNA yield was quantified by spectrophotometric analysis and quality was verified on gel electrophoresis. Total RNA (3 μg) was used in the first-strand cDNA synthesis with T7-Oligo (dT) primer and SuperScript II reverse transcriptase (Life Technologies). The second-strand cDNA synthesis was done using One-Cycle cDNA Synthesis Kit (Affymetrix). The double-stranded cDNA was purified using sample cleanup modules and served as a template in the subsequent *in vitro* transcription reaction for complementary RNA (cRNA) amplification and biotin labeling. The biotinylated cRNA (20 μg) was fragmented and hybridized with pre-equilibrated HG-U133 Plus 2.0 Affymetrix GeneChip for 16 h at 45 °C. HG-U133 Plus 2.0 Affymetrix GeneChip contains more than 54,000 probe sets representing approximately 38,500 genes (estimated by UniGene coverage). After the hybridization cocktails were removed, the chips were washed and stained. The chips were scanned with a ChipScanner 3000 (Affymetrix) to detect hybridization signals. Scanned image output files were visually examined in order to detect major chip defects and hybridization artifacts, and then analyzed with Affymetrix GeneChip Operating software (GCOS). GCOS generates a detection *p* value from probe pair intensities and assigns a present (*P*), marginal (*M*), or absent (*A*) call to each probe set. We applied the default cut-off value of 0.04 (i.e., a *p* value under 0.04 indicates a *P* call). The normalized data were analyzed with Microsoft Excel and Gene Spring GX 7.3 software (Agilent Technologies).

Autophosphorylation and GST-SAMS phosphorylation assay. PLC/PRF/5 cells were transfected with the empty vector p3xFLAG-CMV, the wild-type SNARK expression vector, or the ^{68}AAAR^{71} expression vector, and incubated for 24 h. The cell lysates and the 6% polyethylene glycol (PEG6000) precipitates were prepared, as described previously [15]. PLC/PRF/5 cells stably expressing SNARK were treated with 1 mM AICAR or glucose-deprivation and cultured for 1 h. Cells were lysed and immunoprecipitated using anti-FLAG M2 Affinity Gel (Sigma). An autophosphorylation assay was performed with the PEG precipitates. The precipitates were incubated for 15 min at 30 °C in kinase assay buffer (15 mM Hepes, pH 7.0, 100 mM NaCl, 1% Triton X-100, 10% glycerol, 15 mM $MnCl_2$, 15 mM $MgCl_2$, and 0.3 mM DTT) with 10 μCi of [γ-^{32}P]ATP [16]. The precipitates were also used for the kinase assay using SAMS peptide fused to glutathione *S*-transferase (GST-SAMS). GST-SAMS was prepared, as described previously [15]. The precipitates were incubated for 15 min at 30 °C in kinase assay buffer with 20 μg of GST-SAMS and 10 μCi of [γ-^{32}P]ATP. These samples were subjected to 10% SDS–PAGE. Radioactivity was detected by autoradiography using FLA-7000 (Fujifilm).

Results and discussion

SNARK was distributed predominantly in the nucleus

To determine the subcellular localization of SNARK, a plasmid vector expressing FLAG-tagged SNARK were transfected into a human hepatocellular carcinoma-derived cell line PLC/PRF/5. Exogenous proteins were detected using indirect immunofluorescence. The majority of SNARK was localized in the nucleus (Fig. 1A). A similar nuclear distribution of exogenous SNARK protein was also seen in a human cancer-derived cell lines HeLa (Fig. 1A). To confirm the subcellular localization of endogenous SNARK, subcellular fractionation was carried out followed by detection of SNARK by Western blot. Endogenous SNARK was also mainly present in the nuclear fraction of both PLC/PRF/5 cells and HeLa cells (Fig. 1B). C23 and HSP90 were used as markers of the nuclear and cytosolic fractions, respectively.

SNARK was constitutively distributed in the nucleus

To ask whether the subcellular localization of SNARK is altered by various stimuli, SNARK overexpressing cells were treated by

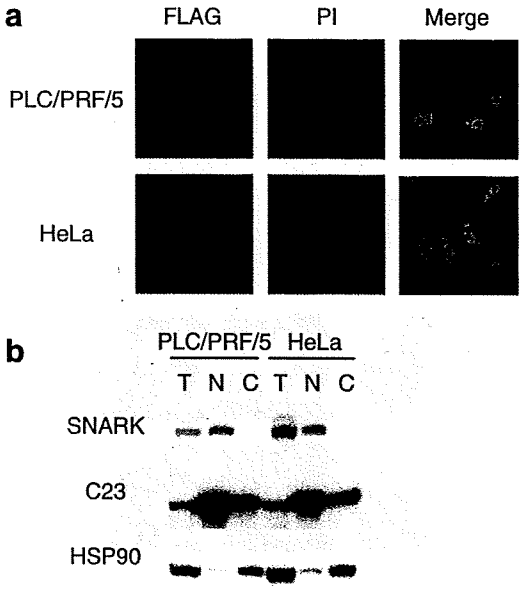

Fig. 1. Subcellular localization of SNARK. (a) Confocal microscopy of PLC/PRF/5 cells transiently expressing FLAG-SNARK. Green, FLAG-tagged proteins immunostained with anti-FLAG M2 antibody. Red, Nuclei visualized by counter-staining DNA with PI. Original magnification, 630×. (b) Immunoblot of the cytosolic and nuclear fractions from PLC/PRF/5 cells. Equal amounts (10 μg) of nuclear (N), cytosolic (C), and total (T) extracts from PLC/PRF/5 were analyzed by 10% SDS–PAGE. C23 and HSP90 were used as markers of the nuclear and cytosolic fractions, respectively.

1 mM AICAR, a representative AMPK activator, and glucose-deprivation which is known to activate SNARK [12]. As expected, overexpressed SNARK showed enhanced activity against SAMS peptides (Fig. 2A). Subcellular fractionation and Immunofluorescent detection of SNARK demonstrated that most of SNARK stay in the nucleus under these stimuli (Fig. 2B and C).

Identification of a functional nuclear localization signal in SNARK

To explore the mechanism of the preferential nuclear localization of SNARK, potential NLS motifs were searched among the amino acid sequences of SNARK. The minimum requirement for a monopartite NLS is Lys-Lys/Arg-X-Lys/Arg (K-K/R-X-K/R) [17,18]. Three candidate sequences, ^{68}KKAR^{71}, ^{375}KKSR^{378}, and ^{450}KKPR^{453} were predicted based on the amino acid sequences of human SNARK. To identify the functional NLS in SNARK, a series of constructs expressing deletion mutants with FLAG-tag were prepared (Supplementary Figure 1a). The expression of each mutant was confirmed using immunoblotting (Supplementary Figure 1b). The subcellular localization of the series of transiently expressed mutant proteins was determined using immunofluorescence. FLAG-SNARK-(2–447), FLAG-SNARK-(2–370), and FLAG-SNARK-(2–169), which contain ^{68}KKAR^{71}, exhibited apparent nuclear localization, whereas FLAG-SNARK-(78–447), FLAG-SNARK-(311–628), and FLAG-SNARK-(390–628), each of which lacked ^{68}KKAR^{71}, were localized predominantly in the cytoplasm (Fig. 3). These results suggest that ^{68}KKAR^{71} functions as a NLS motif in SNARK. On the other hand, the presence or the absence of ^{375}KKSR^{378} and ^{450}KKPR^{453} did not affect the localization of mutant proteins.

To determine whether ^{68}KKAR^{71} functions as a NLS, site-directed mutagenesis of this motif was performed. The first two core lysine residues of ^{68}KKAR^{71} were altered to alanine (^{68}AAAR^{71}) (Supplementary Figure 2a). The expression of this mutant was confirmed by Immunoblotting (Supplementary Figure 2b). The resulting mutant protein exhibited a significantly altered localization. The ^{68}AAAR^{71}-mutant was mainly localized in the cytoplasm and small part of proteins remained in the nucleus (Fig. 4A). The distributions of wild-type and ^{68}AAAR^{71}-mutant SNARK proteins were evaluated in at least 300 transfected cells. Wild-type SNARK was dominantly localized in the nucleus in about 90% of the cells, whereas ^{68}AAAR^{71}-mutant was localized mainly in the cytoplasm and partially in the nucleus (Fig. 4B). Thus, ^{68}KKAR^{71} was necessary for the localization of SNARK in the nucleus. Since the kinase activity of ^{68}AAAR^{71}-mutant was as high as that of wild-type SNARK, kinase activity of SNARK was not indispensable for the nuclear localization (Fig. 4C).

To further confirm the NLS function, the N-terminal 169 amino acid-length fragment of SNARK containing ^{68}KKAR^{71} was fused to GFP (Supplementary Figure 2c). The expression of this mutant was confirmed by Immunoblotting (Supplementary Figure 2d). SNARK-(1–169)-GFP was localized predominantly in the nucleus,

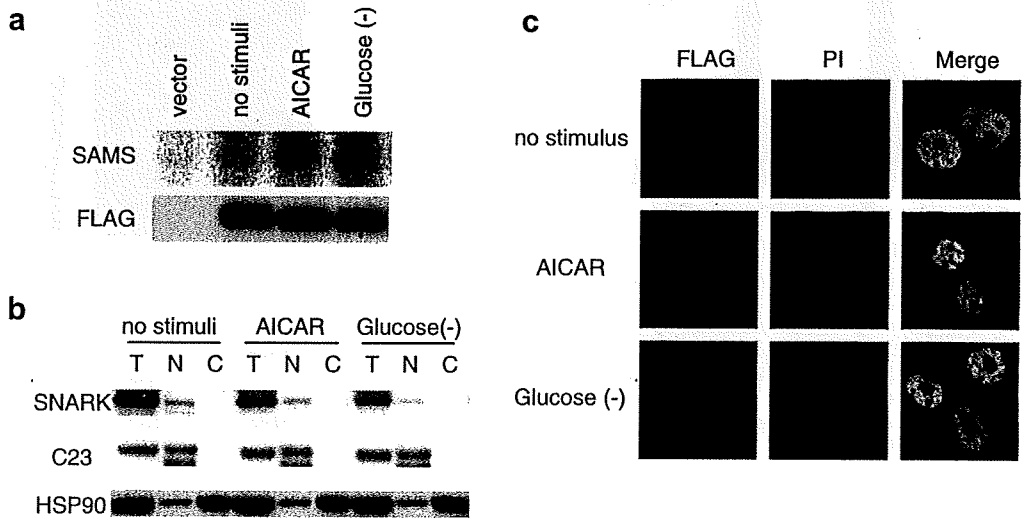

Fig. 2. The association between the activation and localization in SNARK. (a) *In vitro* kinase assay of SNARK stimulated by AICAR and glucose-deprivation. The immunoprecipitants of FLAG-SNARK were prepared from lysates of SNARK expressing PLC/PRF/5 cells treated with 1 mM AICAR or glucose-deprivation for an hour and used to perform a kinase assay with GST-SAMS as substrate. Upper panel indicates *in vitro* kinase assay, and lower panel indicates anti-FLAG immunoblot, respectively. (b) Immunoblot of the cytosolic and nuclear fractions from PLC/PRF/5 cells. Equal amounts (10 μg) of nuclear (N), cytosolic (C), and total (T) extracts from PLC/PRF/5 treated with indicated stimuli were analyzed by 10% SDS–PAGE. C23 and HSP90 were used as markers of the nuclear and cytosolic fractions, respectively. (c) Confocal microscopy of cells expressing FLAG-SNARK. PLC/PRF/5 cells expressing FLAG-SNARK were treated with indicated stimuli. Green, FLAG-SNARK immunostained with anti-FLAG M2 antibody. Red, nuclei visualized by counter-staining DNA with PI. Original magnification, 630×.

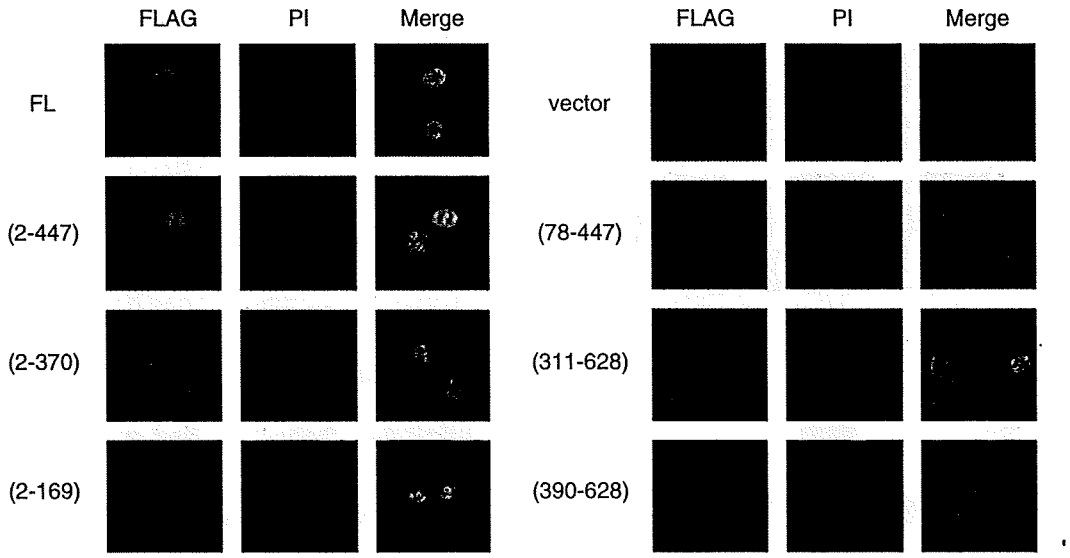

Fig. 3. Subcellular localization of FLAG-tagged deletion mutants of SNARK. Confocal microscopy of PLC/PRF/5 cells expressing FLAG-tagged SNARK deletion mutants showing subcellular localization. Green, wild-type and deletion mutants of SNARK immunostained with anti-FLAG M2 antibody. Red, Nuclei visualized by counter-staining DNA with PI. Original magnification, 630×.

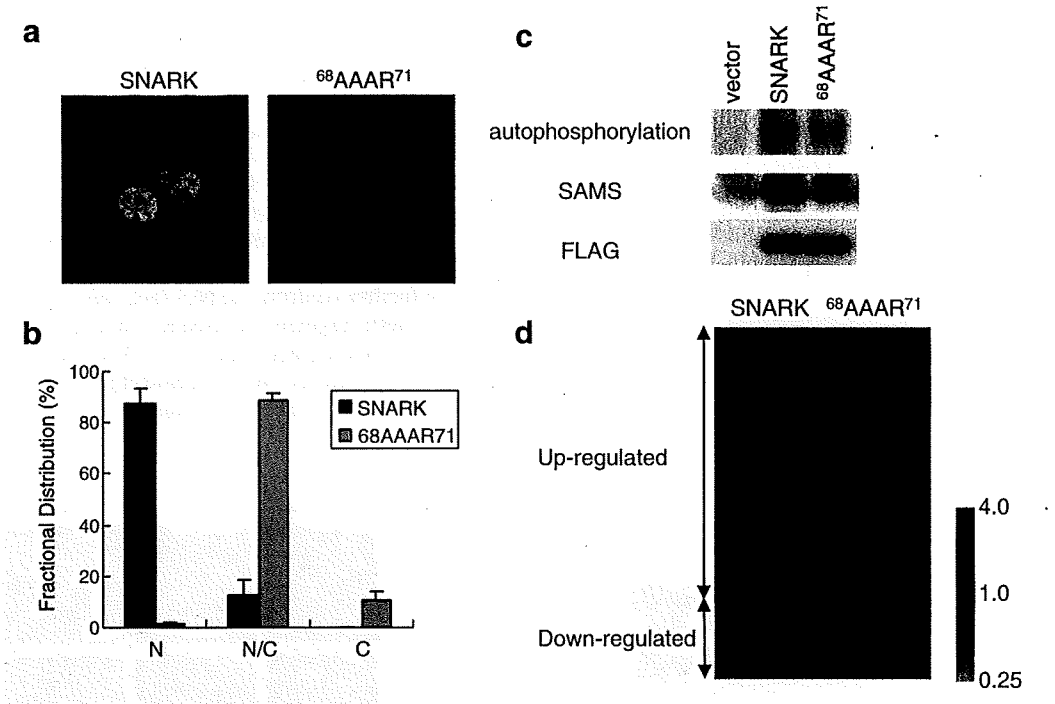

Fig. 4. Identification of a functional NLS in SNARK. (a) Confocal microscopy of cells expressing ^{68}AAAR^{71}-mutant SNARK. Green, wild-type and mutant SNARK immunostained with anti-FLAG M2 antibody. Red, nuclei visualized by counter-staining DNA with PI. Original magnification, 630×. (b) Bar graphs (mean ± SE; $n = 3$) representing the localization of FLAG-SNARK and FLAG-^{68}AAAR^{71} determined in over 300 cells transfected with each plasmid. N; predominantly nuclear localization; N/C, nuclear/cytoplasmic localization; C, predominantly cytoplasmic localization. (c) *In vitro* kinase assay of SNARK or ^{68}AAAR^{71}-mutant SNARK. The PEG precipitants of SNARK and ^{68}AAAR^{71}-mutant SNARK were prepared from lysates of transiently transfected PLC/PRF/5 cells and used to perform a kinase assay with GST-SAMS as substrate. Upper panel indicates an autophosphorylation assay, middle panel indicates *in vitro* kinase assay, and lower panel indicates anti-FLAG immunoblot, respectively. (d) Expression of the probe sets up-regulated more than 1.5-fold and down-regulated less 0.67 by SNARK. Relative expression in the wild-type or ^{68}AAAR^{71}-mutant SNARK expressing cells standardized by the expression in vector-transfected cells was visualized.

whereas GFP without the NLS was distributed in both the nucleus and the cytoplasm (Supplementary Figure 2e).

The NLS motif that we identified above is conserved among all reported orthologs, including those in chimpanzee, cattle, mouse, rat, and chicken (Supplementary Figure 2f).

In these results, SNARK constitutively resided in the nucleus and was activated by AICAR and glucose-deprivation. AICAR and glucose-deprivation increase the cellular AMP:ATP ratio [1]. AMPK and AMPK-related kinases are believed to be activated by increased AMP:ATP ratio through direct activation mechanism of allosteric effect and/or indirectly activated by phosphorylation at threonine residue in the activation loop by upstream kinases, LKB1, CaMKK, and TAK1 [19]. CaMKK and TAK1 are to be localized in the cytoplasm, but LKB1 is localized in both nucleus and cyto-

plasm [20–22]. Therefore SNARK might be phosphorylated by LKB1 in the nucleus. It is possible that SNARK might form a complex with LKB1 or other AMPKK in the nucleus, but this remains to be determined.

The gene expression alterations by overexpressed SNARK

As SNARK was localized in the nucleus, we considered that SNARK might regulate cell cycle or gene expression. There was no significant difference in cell growth between PLC/PRF/5 cells stably expressing SNARK and vector control (data not shown). To evaluate that SNARK modulates gene expression in the nucleus, we compared the gene expression profiles of SNARK overexpressing PLC/PRF/5 cells to NLS mutant SNARK (^{68}AAAR^{71}) expressing PLC/PRF/5 cells and vector-transfected PLC/PRF/5 cells. Among 54,000 probe sets on the HG-U133 Plus 2.0 Affymetrix GeneChip, 20,308 probe sets were assigned for "present" in all the samples from vector, wild-type and ^{68}AAAR^{71}-mutant SNARK transfected cells.

First, to assess whether SNARK modulates gene expression, we compared the expression profiles of SNARK overexpressing cells with those of vector-transfected cells. We identified 945 (739 up-regulated and 206 down-regulated) probe sets with more than 1.5-fold change in expression. This indicated that SNARK altered the gene expression. Second, to identify that SNARK functions as a transcriptional modulator in the nucleus but not the cytoplasm, we examined the expression profiles of ^{68}AAAR^{71} overexpressing cells compared with those of vector-transfected cells (Fig. 4D). Among the 739 up-regulated probe sets by overexpressed SNARK, only 187 probe sets increased more than 1.5-fold in ^{68}AAAR^{71} overexpressing cells. In parallel, among the 206 down-regulated probe sets by overexpressed SNARK, only 67 probe sets decreased more than 1.5-fold in ^{68}AAAR^{71} overexpressing cells. Similarly we identified 108 (76 up-regulated and 32 down-regulated) probe sets with more than 2.0-fold change in SNARK overexpressing cells compared with vector-transfected cells (Supplementary Table 2). Among the 76 up-regulated probe sets by overexpressed SNARK, only eight probe sets increased more than 2.0-fold in ^{68}AAAR^{71} overexpressing cells compared with vector-transfected cells. On the other hand, among the 32 down-regulated probe sets by overexpressed SNARK, only 13 probe sets decreased more than 2.0-fold in ^{68}AAAR^{71} overexpressing cells compared with vector-transfected cells. Thus, overexpressed SNARK altered the gene expression profiles more than ^{68}AAAR^{71}. This result implied that SNARK in the nucleus but not the cytoplasm had a remarkable impact on the gene expression.

In this study, SNARK is localized in the nucleus and affects gene expression profiles. These results indicate that SNARK can work as a transcriptional modulator working in the nucleus in response to stress. Among 76 probe sets with more than 2.0-fold increase in PLC/PRF/5 cells overexpressing SNARK, nine probe sets also detected more than 2.0-fold increase in a human pancreatic cancer cell line PANC-1 under glucose-deprivation (our unpublished data). This concordance of induced genes between the overexpression of SNARK and glucose-deprivation well consists with the activation of SNARK under glucose-deprivation.

The present study demonstrates for the first time, to our knowledge, the alteration of gene expression profiles by SNARK. This information may be the platform to elucidate the molecular mechanism and the physiological signification of SNARK.

Acknowledgments

This work was supported by Grants for the Third-Term Comprehensive 10-Year Strategy for Cancer Control, and a Grant-in-Aid for Cancer Research from the Ministry of Health, Labour and Welfare and a Grant-in-Aid for Scientific Research on Priority Areas from the Ministry of Education, Culture, Sports, Science and Technology, Japan.

Appendix A. Supplementary data

Supplementary data associated with this article can be found, in the online version, at doi:10.1016/j.bbrc.2008.10.143.

References

[1] B.B. Kahn, T. Alquier, D. Carling, D.G. Hardie, AMP-activated protein kinase: ancient energy gauge provides clues to modern understanding of metabolism, Cell Metab. 1 (2005) 15–25.
[2] D.G. Hardie, S.A. Hawley, J.W. Scott, AMP-activated protein kinase–development of the energy sensor concept, J. Physiol. 574 (2006) 7–15.
[3] D.G. Hardie, D. Carling, M. Carlson, The AMP-activated/SNF1 protein kinase subfamily: metabolic sensors of the eukaryotic cell?, Annu Rev. Biochem. 67 (1998) 821–855.
[4] B.E. Kemp, K.I. Mitchelhill, D. Stapleton, B.J. Michell, Z.P. Chen, L.A. Witters, Dealing with energy demand: the AMP-activated protein kinase, Trends Biochem. Sci. 24 (1999) 22–25.
[5] A.M. Turnley, D. Stapleton, R.J. Mann, L.A. Witters, B.E. Kemp, P.F. Bartlett, Cellular distribution and developmental expression of AMP-activated protein kinase isoforms in mouse central nervous system, J. Neurochem. 72 (1999) 1707–1716.
[6] I. Salt, J.W. Celler, S.A. Hawley, A. Prescott, A. Woods, D. Carling, D.G. Hardie, AMP-activated protein kinase: greater AMP dependence, and preferential nuclear localization, of complexes containing the alpha2 isoform, Biochem. J. 334 (Pt. 1) (1998) 177–187.
[7] M. Kodiha, J.G. Rassi, C.M. Brown, U. Stochaj, Localization of AMP kinase is regulated by stress, cell density, and signaling through the MEK–>ERK1/2 pathway, Am. J. Physiol. Cell Physiol. 293 (2007) C1427–C1436.
[8] A. Suzuki, S. Okamoto, S. Lee, K. Saito, T. Shiuchi, Y. Minokoshi, Leptin stimulates fatty acid oxidation and peroxisome proliferator-activated receptor alpha gene expression in mouse C2C12 myoblasts by changing the subcellular localization of the alpha2 form of AMP-activated protein kinase, Mol. Cell. Biol. 27 (2007) 4317–4327.
[9] J.M. Lizcano, O. Goransson, R. Toth, M. Deak, N.A. Morrice, J. Boudeau, S.A. Hawley, L. Udd, T.P. Makela, D.G. Hardie, D.R. Alessi, LKB1 is a master kinase that activates 13 kinases of the AMPK subfamily, including MARK/PAR-1, EMBO J. 23 (2004) 833–843.
[10] G. Manning, D.B. Whyte, R. Martinez, T. Hunter, S. Sudarsanam, The protein kinase complement of the human genome, Science 298 (2002) 1912–1934.
[11] D.L. Lefebvre, Y. Bai, N. Shahmolky, M. Sharma, R. Poon, D.J. Drucker, C.F. Rosen, Identification and characterization of a novel sucrose-non-fermenting protein kinase/AMP-activated protein kinase-related protein kinase, SNARK, Biochem. J. 355 (2001) 297–305.
[12] D.L. Lefebvre, C.F. Rosen, Regulation of SNARK activity in response to cellular stresses, Biochim. Biophys. Acta 1724 (2005) 71–85.
[13] K. Tsuchihara, T. Ogura, R. Fujioka, S. Fujii, W. Kuga, M. Saito, T. Ochiya, A. Ochiai, H. Esumi, Susceptibility of Snark-deficient mice to azoxymethane-induced colorectal tumorigenesis and the formation of aberrant crypt foci, Cancer Sci. 99 (2008) 677–682.
[14] A. Suzuki, G. Kusakai, A. Kishimoto, Y. Minegichi, T. Ogura, H. Esumi, Induction of cell–cell detachment during glucose starvation through F-actin conversion by SNARK, The fourth member of the AMP-activated protein kinase catalytic subunit family, Biochem. Biophys. Res. Commun. 311 (2003) 156–161.
[15] A. Kishimoto, T. Ogura, H. Esumi, A pull-down assay for 5′ AMP-activated protein kinase activity using the GST-fused protein, Mol. Biotechnol. 32 (2006) 17–21.
[16] P. Legembre, R. Schickel, B.C. Barnhart, M.E. Peter, Identification of SNF1/AMP kinase-related kinase as an NF-kappaB-regulated anti-apoptotic kinase involved in CD95-induced motility and invasiveness, J. Biol. Chem. 279 (2004) 46742–46747.
[17] M.R. Hodel, A.H. Corbett, A.E. Hodel, Dissection of a nuclear localization signal, J. Biol. Chem. 276 (2001) 1317–1325.
[18] S.W. Leung, M.T. Harreman, M.R. Hodel, A.E. Hodel, A.H. Corbett, Dissection of the karyopherin alpha nuclear localization signal (NLS)-binding groove: functional requirements for NLS binding, J. Biol. Chem. 278 (2003) 41947–41953.
[19] T. Williams, J.E. Brenman, LKB1 and AMPK in cell polarity and division, Trends Cell Biol. 18 (2008) 193–198.
[20] J. Nezu, A. Oku, M. Shimane, Loss of cytoplasmic retention ability of mutant LKB1 found in Peutz-Jeghers syndrome patients, Biochem. Biophys. Res. Commun. 261 (1999) 750–755.
[21] S.M. Lemrow, K.A. Anderson, J.D. Joseph, T.J. Ribar, P.K. Noeldner, A.R. Means, Catalytic activity is required for calcium/calmodulin-dependent protein kinase IV to enter the nucleus, J. Biol. Chem. 279 (2004) 11664–11671.
[22] K. Deacon, J.L. Blank, Characterization of the mitogen-activated protein kinase kinase 4 (MKK4)/c-Jun NH2-terminal kinase 1 and MKK3/p38 pathways regulated by MEK kinases 2 and 3. MEK kinase 3 activates MKK3 but does not cause activation of p38 kinase in vivo, J. Biol. Chem. 272 (1997) 14489–14496.

Biochemical and Biophysical Research Communications 380 (2009) 171–176

Contents lists available at ScienceDirect

Biochemical and Biophysical Research Communications

journal homepage: www.elsevier.com/locate/ybbrc

Inhibitors of insulin-like growth factor-1 receptor tyrosine kinase are preferentially cytotoxic to nutrient-deprived pancreatic cancer cells

Isao Momose *, Setsuko Kunimoto, Michiyo Osono, Daishiro Ikeda

Numazu Bio-Medical Research Institute, Microbial Chemistry Research Center, 18-24 Miyamoto, Numazu, Shizuoka 410-0301, Japan

ARTICLE INFO

Article history:
Received 8 January 2009
Available online 21 January 2009

Keywords:
IGF-1R
IGF-1R kinase inhibitor
AG1024
Nutrient starvation
Pancreatic cancer

ABSTRACT

Chronic deprivation of nutrients is rare in normal tissues, however large areas of tumor are nutrient-starved and hypoxic due to a disorganized vascular system. Some cancers show an inherent ability to tolerate severe growth conditions. Therefore, we screened chemical compounds to identify cytotoxic agents that function preferentially in nutrient-deprived conditions. We found that AG1024, a specific inhibitor of insulin-like growth factor-1 receptor tyrosine kinase (IGF-1R), showed preferential cytotoxicity to human pancreatic cancer cells in nutrient-deprived conditions relative to cells in nutrient-sufficient conditions. The cytotoxicity of I-OMe-AG538 (another specific inhibitor of IGF-1R kinase) was also enhanced in nutrient-deprived cells. In addition, AG1024 and I-OMe-AG538 potently inhibited IGF-1R activation to nutrient-deprived cells. In contrast, conventional chemotherapeutic drugs, as well as inhibitors of PDGFR and EGFR kinases, elicited weak cytotoxicity. These data indicate that nutrient-deprived human pancreatic cancer cells have increased sensitivity to inhibition of IGF-1R activation. IGF-1R inhibitors offer a promising strategy for anticancer therapeutic approaches that are oriented toward tumor microenvironment.

Patients diagnosed with pancreatic cancer, an aggressive disease with the lowest 5-year survival rates of all cancers, develop metastases rapidly and die within a short period of time after diagnosis [1,2]. Pancreatic cancer is largely resistant to almost all known chemotherapeutic agents, including 5-fluorouracil, paclitaxel and doxorubicin; surgery is the only current treatment modality that offers any prospect of potential cure. Clearly, there is a dire need for new therapeutic alternatives that improve clinical outcome for pancreatic cancer patients.

Tumor microenvironment exerts an important influence on cancer physiology. The disorganized vascular system in a tumor often results in large areas of tumor starved for nutrients and oxygen. Pancreatic cancers in particular, which are characterized as hypovascular tumors, show an inherent ability to tolerate severe growth conditions. Certain human pancreatic cancer cell lines, including PANC-1, AsPC-1, BxPC-3 and KP-3, exhibit marked environmental tolerance and can survive for prolonged periods of time in nutrient-deprived conditions. Because tolerance of these cancer cells to nutrient starvation has been associated with the activity of protein kinase B (PKB)/Akt [3], it has been hypothesized that agents that diminish such tolerance could function as anticancer agents [4–7].

Insulin-like growth factors-1 (IGF-1) and -2 (IGF-2) are involved in the pathophysiology of a wide range of human neoplasias due to the mitogenic and antiapoptotic properties mediated by their type 1 receptor (IGF-1R) [8]. IGF-1R is a tetrameric transmembrane receptor tyrosine kinase composed of two α and β subunits. The extracellular α subunit is responsible for ligand binding, whereas the β subunit consists of a transmembrane domain and an intracellular tyrosine kinase domain [9,10]. Ligand binding activates the intrinsic receptor tyrosine kinase, resulting in trans-β subunit autophosphorylation and stimulation of PI3K-AKT-TOR and RAF-MAPK signaling pathways. In addition to cell proliferation, activation of IGF-1R has been reported to stimulate cell survival, transformation, metastasis and angiogenesis [11]. Targeted inhibition of IGF-1R signaling has been shown to result in impressive anti-neoplastic activity in many *in vitro* and *in vivo* models of common human cancers. IGF-1R small interfering RNAs [12], anti-receptor antibodies [13,14], a IGF-1-like competitive peptide antagonist [15], a dominant-negative IGF-1R [16–18] and small-molecule IGF-1R tyrosine kinase inhibitors [19,20] have all been found to interfere with cell growth and proliferation. IGF-1R is therefore regarded as an attractive potential target in the development of new drugs to treat malignant tumors.

In this study, we screened chemical compounds to identify agents that preferentially reduce the survival of nutrient-deprived human pancreatic cancer PANC-1 cells. The screen identified IGF-1R inhibitors, which function as cytotoxic agents preferentially on human pancreatic cancer cells in nutrient-deprived conditions.

* Corresponding author. Fax: +81 55 922 6888.
E-mail address: imomose@bikaken.or.jp (I. Momose).

0006-291X/$ - see front matter © 2009 Elsevier Inc. All rights reserved.
doi:10.1016/j.bbrc.2009.01.065

Materials and methods

Materials. Antibodies used in Western blotting included anti-IGF-1Rβ (sc-713), anti-Erk 1 (sc-93) and anti-phospho-Erk (sc-7383) from Santa Cruz Biotechnology (Santa Cruz, CA); anti-α-tubulin (T5168) from Sigma–Aldrich (St. Louis, MO); and anti-Akt (#9272), anti-phospho-Akt (Ser 473) (#9271), anti-phospho-Akt (Thr 308) (#9275) and anti-phospho-IGF-1R (#3021) from Cell Signaling Technology (Denvers, MA). Recombinant human IGF-1 was from R&D Systems (Minneapolis, MN). AG1024, AG1296, AG1478 and I-OMe-AG538 were obtained from Calbiochem (Madison, WI). Doxorubicin hydrochloride, fluorouracil, paclitaxel and mitomycin C were from Sigma. The SCADS inhibitor kit I consisting of 79 chemical inhibitors with ~60 different targets was kindly provided by the Screening Committee on Anticancer Drugs (Japan).

Cells and culture. Human pancreatic cancer cell lines PANC-1, Capan-1, MIA Paca-2, BxPC-3 and PSN-1 were obtained from the American Type Culture Collection (Rockville, MD). Cells were grown at 37 °C with 5% CO_2 in Dulbecco's modified Eagle medium (DMEM; Nissui, Tokyo, Japan) supplemented with 10% fetal bovine serum (FBS; Tissue Culture Biologicals, Tulare, CA), 100,000 U/L penicillin G, and 100 mg/L streptomycin. Nutrient starvation was achieved by culturing the cells in nutrient-deprived medium (NDM) as previously described [3–7]. Briefly, the composition of the NDM was as follows: 265 mg/L $CaCl_2{\cdot}H_2O$, 400 mg/L KCl, 200 mg/L $MgSO_4{\cdot}7H_2O$, 6400 mg/L NaCl, 163 mg/L $NaH_2PO_4{\cdot}2H_2O$, 0.1 mg/L $Fe(NO_3)_3{\cdot}9H_2O$, 5 mg/L phenol red, 100,000 U/L penicillin G, 100 mg/L streptomycin, 25 mmol/L HEPES buffer (pH 7.4), and MEM vitamin solution (Invitorogen, Carlsbad, CA); the final pH was adjusted to 7.4 with 10% $NaHCO_3$.

Preferential cytotoxicity in nutrient-deprived conditions. PANC-1 cells (2.5×10^4 cells/well) in 96-well plates were cultured in DMEM for 24 h. The cells were washed with PBS and the medium was replaced with either fresh DMEM or NDM. Test samples were added to the well and cells were cultured for 24 h. Cytotoxicity was determined using the MTT assay [21].

Preparation of cell lysate and Western blotting. PANC-1 cells (5×10^5) in 35-mm dishes were incubated in DMEM for 24 h. The cells were washed with PBS and the medium was replaced with either fresh DMEM or NDM. AG1024 or I-OMe-AG538 was added to each dish and the cells were incubated for 1 h prior to stimulation with 50 ng/ml IGF-1 for 10 min. The cells were washed twice with ice-cold PBS containing 100 μm Na_3VO_4 and then lysed in a lysis buffer (20 mM *N*-2-hydroxyethylpiperazine-*N'*-2-ethanesulfonic acid, 150 mM NaCl, 1% Triton X-100, 10% glycerol, 1 mM EDTA, 50 mM NaF, 50 mM β-glycerolphosphate, 1 mM Na_3VO_4, pH 7.5, and 25 μg/ml each of antipain, leupeptin, and pepstatin). Equal amounts of protein extract were separated by SDS–polyacrylamide gel electrophoresis, transferred onto Immobilon polyvinylidene difluoride membranes (Millipore, Bedford, MA) and probed with anti-IGF-1R, anti-phospho-IGF-1R, anti-Akt, anti-phospho-Akt (Thr 308), anti-phospho-Akt (Ser 473), anti-Erk 1,

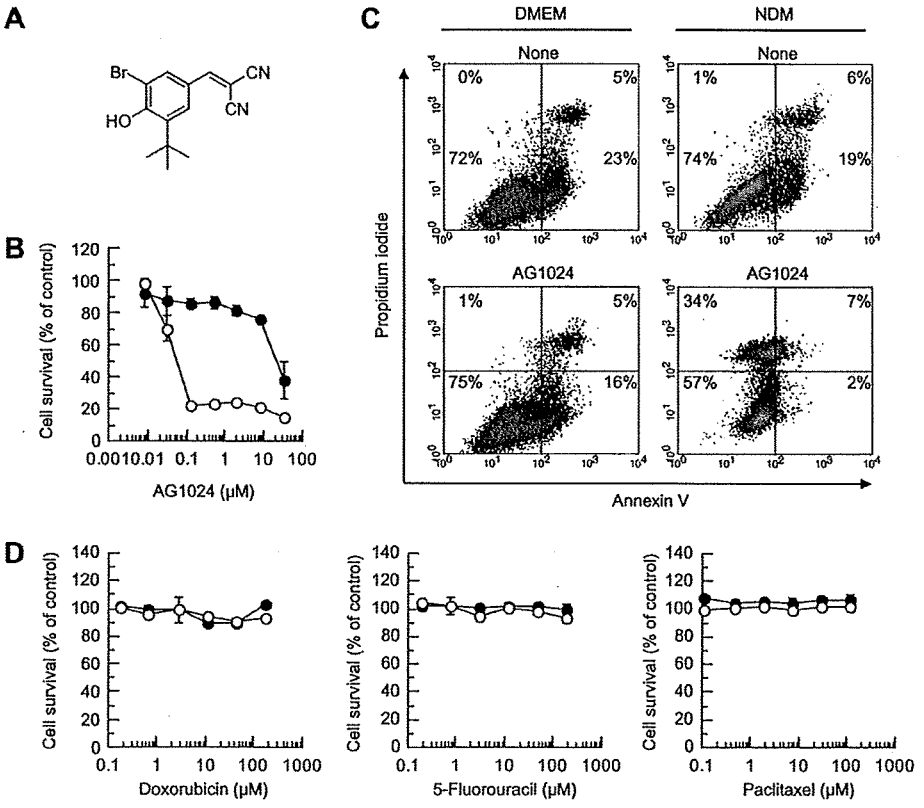

Fig. 1. Effect of AG1024 on survival of PANC-1 cells in nutrient-deprived conditions. (A) Structure of AG1024. (B) Effect of AG1024 on PANC-1 cell viability in normal medium, DMEM (●) and nutrient-deprived medium, NDM (○). PANC-1 cells incubated in DMEM for 24 h. The cells were then washed with PBS and the medium was replaced with either fresh DMEM or NDM. The indicated concentrations of AG1024 were added to each well and the cells were incubated for 24 h. Cell viability was determined using the MTT assay. (C) Flow cytometric analysis of AG1024-treated PANC-1 cells. PANC-1 cells were cultured with 0.3 μM AG1024 in DMEM or NDM for 12 h. The cells were stained with annexin V-FITC and propidium iodide according to instructions for the apoptosis detection kit and then analyzed using a flow cytometer. (D) Effect of conventional anticancer drugs on survival of PANC-1 cells in nutrient-deprived conditions. PANC-1 cells were incubated with indicated concentrations of doxorubicin, 5-fluorouracil and paclitaxel in DMEM (●) or NDM (○) for 24 h.